Dong, S., Zhou, W., Liu, Q., Wang, H. & Ji, Y. (2021): Impact of Open Pit Mining on Karst Springs. – In: Dong, S., Zhou, W., Liu, Q., Wang, H. & Ji, Y. (eds): Methods and Techniques for Preventing and Mitigating Water Hazards in Mines. – p. 387–466, 27 Abb., 11 Tab.; Cham (Springer).

Chapter 9
Impact of Open Pit Mining on Karst Springs

9.1 Introduction

Much of the mining and quarrying conducted in karst areas is for the rock itself. Some carbonate rocks contain valuable supplies of water, oil, and gas. They may weather to form bauxite deposits and host ore deposits such as lead, zinc, iron, and gold. Coal is often found within thick carbonate sequences, while diamond-bearing kimberlitic pipes may penetrate through them. To the mining industry, caves, sinkholes, and conduits are nuisance to their operations and lost revenue. Presence of karst often mean extra costs for stripping, lost drill steel during blast-hole drilling, reserves that disappear as caves are encountered, non-spec fines in the aggregate, flooded quarries, high pumping costs, and machinery damage and possible personal injury as caverns collapse or ground settles under mobile equipment. To the people living adjacent to quarries, mining means noise, dust, possible water loss and contamination. It is not uncommon that dry wells and springs, destruction of caves with endangered species, or structure damage caused by sinkhole formation lead to lawsuits. Many limestone quarries are located and engineered to attempt to reduce the karst-related problems to a minimum. Because each karst aquifer is unique, the exact inter-relationship between a mining operation and a karst aquifer can only be established by site-specific circumstances.

The geotechnical and environmental impacts are generally more significant when mining occurs below the groundwater level. Mining can create relatively abrupt and unnatural hydraulic gradients in the surrounding area by forming an open space beneath the natural piezometric surface. Water may slowly flow out of rock into the mine or it may flow into the mine at a rate of hundreds of liters per second if the rock is highly fractured. In many situations, it is necessary to pump the water out of the mine to create a workable condition. Disturbance of the natural water flow by dewatering can intensify the subsurface erosion processes and directly cause ground collapse. In 1949 dewatering in a limestone quarry in Hershey, Pennsylvania, caused more than 100 sinkholes in an area of approximately 2600 ha (Foose 1953). Mine dewatering

S. Dong et al., *Methods and Techniques for Preventing and Mitigating Water Hazards in Mines*, Professional Practice in Earth Sciences,
https://doi.org/10.1007/978-3-030-67059-7_9

produces a cone of depression in the water level contours. The shape of the cone of depression is often irregular and influenced by the hydrogeologic heterogeneity of the aquifer and its boundary conditions. If the cone of depression extends to include surface streams, it is not surprising that surface water loses some of its flow to the mine.

The amount of water flowing into a mine often experiences dynamic changes as the mining progresses. When mining intercepts large water-bearing conduits, the flow rates may increase substantially by an order of magnitude or more in a very short period of time. The flow may be discolored, new seepage entry and exit points may develop, and regional groundwater level may drop suddenly. If the pump capacity is less than the inflow rate, the mine may be completely flooded, and surface manifestations may occur in the form of depressions in embankments and sinkholes in overburden. Sudden, unexpected, significant, and obvious changes to the preexisting hydrogeological regimes characterize such a karst-related flow event. It may also trigger sinkholes within its influence area, and the additional sinkholes may bring more water into the mine, thus further enhancing the subsurface erosion processes. If the intercepted conduits carry majority of the groundwater, mining has the potential to completely change the groundwater flow direction. This occurred in a limestone quarry of Harmony, Minnesota, when quarrying progressed below the water table and intercepted the major conduits. Approximately 90% of the groundwater that formerly discharged from a large spring flows into the quarry (Green et al. 2003).

When groundwater is confined in conduits of a karst aquifer, mining may occur above the water body but below the potentiometric pressure. The competent and impervious limestone rock may act as a hydrologic barrier to temporarily prevent the groundwater from flowing into the mine. As the mining gets deeper, the hydrologic barrier becomes thinner. The pressurized groundwater may break through the barrier through hydrofracturing, and seemingly small modifications to the barrier may cause the inflow. Lolcama et al. (1999) reported such a flooding incident in a limestone quarry in West Virginia. Following a blast, an inflow of approximately 2524 L/s suddenly developed into the floor of the fully operational quarry. The water was traced to originate from a river approximately 460 m away with a head difference of approximately 50 m. The sudden inflow caused a rapid decline of the regional water level in the aquifer, and a water storage basin nearby the river drained rapidly into a sinkhole.

Mining may reactivate old filled karst features. Realization of this possibility is important in evaluating its environmental impacts because the results from traditional geological and hydrogeological investigations may provide misleading information. Boring may indicate clay-filled voids; pumping tests may suggest low hydraulic conductivities of the aquifer. While these findings represent the natural conditions prior to the mine operation, long-term and persistent seepage may eventually result in open channels through features filled with residual clay or other erosional or weathering materials. Abkemeier and Stephenson (2003) reported that a mine in Missouri that had been dry for more than 50 years intercepted a sediment-filled cave system below the water table. The dewatering of the quarry created a flow which eroded the fill, opening a subterranean channel to the Mississippi River. The catastrophic inflow exceeded the pumping capacity and flooded the quarry for over a year, while simultaneously triggering sinkhole collapses in the surrounding area, one of which caused a railroad wreck, diesel spill, and injuries to railroad personnel.

Mining can occur in unsaturated or saturated zone, although defining the peak groundwater level in a karst aquifer is challenging even with several years' groundwater monitoring data. In general, quarrying in the unsaturated zone may result in relatively local impacts such as increased runoff, reduction in temporary storage and potential destruction of hydrologically inactive caves. Exceptions may be those areas with thick unsaturated zone and well-developed epikarst, especially when the mine has a strong hydraulic connection with surface water. The case study presented in this chapter illustrates the methods and techniques that were used to investigate the relationship between a surface mine and a nearby spring as part of a comprehensive environmental impact study.

9.2 Background of Environmental Impact Study

Figure 9.1 shows the location of the study area and general geology. A marble quarry had been in operation from 1964 to 2010. The surface elevation ranged from 1,000 to 1,270 feet above mean sea level (amsl), whereas the bottom of the quarry was at an elevation of approximately 750 feet amsl with seven benches, each bench being approximately 40 feet high. The area in the vicinity of the quarry is heavily forested. To the south of the quarry, relatively steep hills and canyons exist. To the east and north, the topography becomes more moderate and is mantled with light forest and grassland. The environmental impact study was for an application to amend the use permit by expanding the working area of the 80-acre quarry into an adjacent area of approximately 17.1 acres (Fig. 9.1). The purpose of this study was to provide an evaluation of potential geologic, hydrologic, and hydrogeologic environmental impacts and constraints relevant to the proposed project. The proposed quarry expansion had the potential to cause environmental impacts with respect to geologic and hydrogeologic conditions.

The quarry was in an isolated body of marble surrounded by granitic, metamorphic, and sedimentary rocks. Dissolution of the marble rocks along fractures by percolating groundwater has created a localized karst aquifer system of interconnected subterranean channels and caverns that are fed by groundwater inflow from adjacent rock bodies and by percolating surface water and streamflow from above. Surface outflow from the karst aquifer system occurs at springs located in the local creek drainage on the southerly (downslope) side of the marble body. The principal spring, referred to as SP-1, is an important water supply for a nearby city. SP-1 is located approximately 750 feet south of the quarry at an approximate elevation of 588 feet amsl. The terrain at the spring slopes steeply down to the south. It is the outlet of a complex marble aquifer system and discharges from the southern end of the marble at the marble-granodiorite contact.

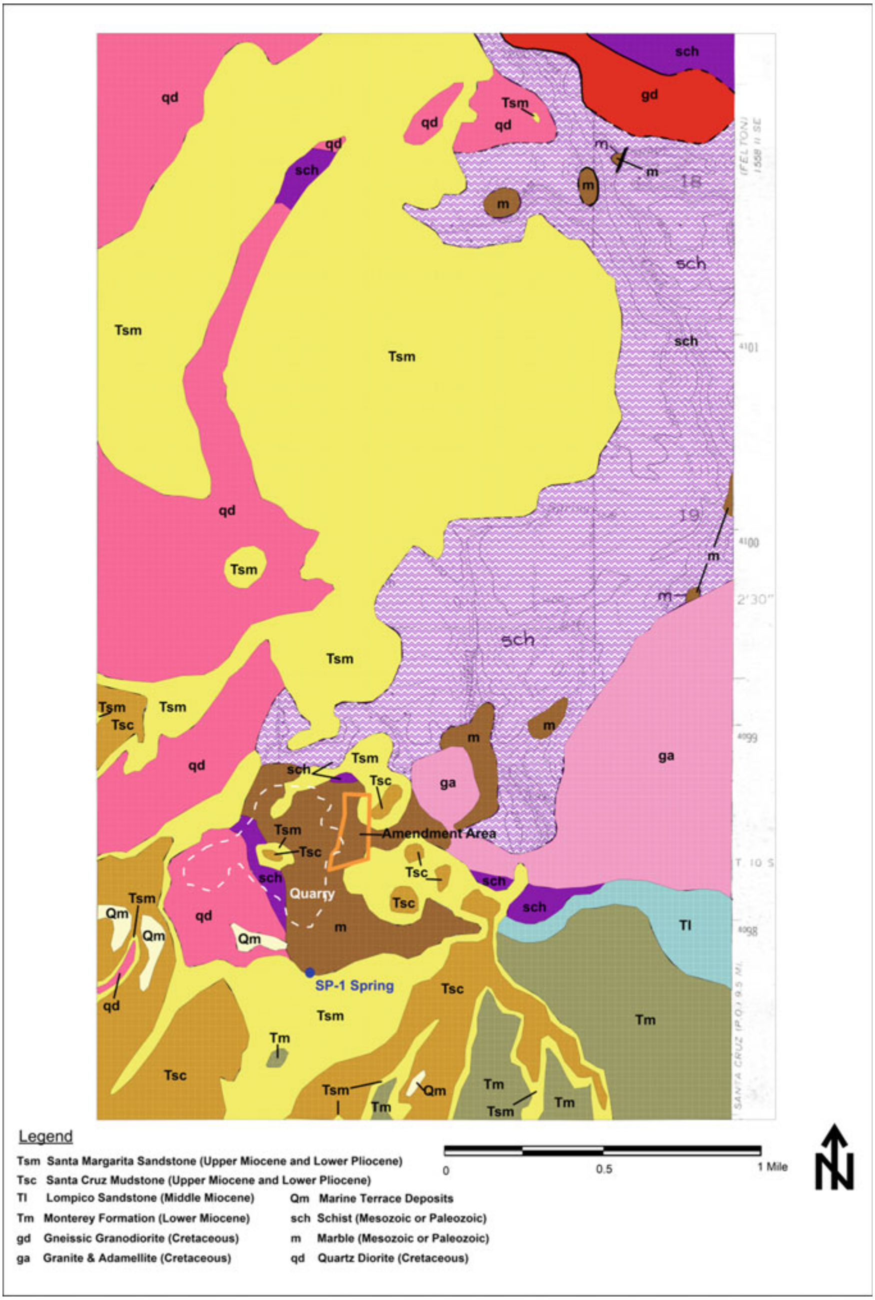

Fig. 9.1 Geology of study area

Environmental concerns associated with the proposed quarry expansion include:

- Quarry blasting could cause additional turbidity in the spring water.
- The expanded quarry activity could potentially alter flow paths in the karst aquifer and reduce flows to SP-1 Spring.
- The changes in surface or subsurface water flow could affect the stability of a landslide adjacent to the spring facility, potentially impacting the turbidity at the spring.
- Extensive grading to remove overburden from the marble deposit in the expansion area and placement of the overburden soils as fill in the existing quarry will expose a considerable area to accelerated erosion, potentially leading to increased turbidity.

9.3 Geologic Setting

The quarry property is situated on the western slope of the central Santa Cruz Mountains, part of the Coast Ranges physiographic province. The northwest-southeast structural grain of the Coast Ranges is controlled by a complex of Pleistocene- and Holocene-active faults within the San Andreas fault system. Southwest of the San Andreas fault, the Coast Ranges, including the Santa Cruz Mountains, are underlain by a large, northwest-trending, fault-bounded, elongate prism of granitic and metamorphic basement rocks. The marble being mined in the quarry is part of a metamorphic rock unit that also includes schist and quartzite. The granitic and metamorphic rock basement is overlain by a sequence of dominantly marine sedimentary rocks of Paleocene to Pliocene age and non-marine sediments of late Pliocene to Pleistocene age.

The study area is tectonically active. The Santa Cruz Mountains are cut by several active faults, of which the San Andreas is the most important. Along the coast, the ongoing tectonic activity is most evident in the formation of the series of uplifted marine terraces that sculpt the southwest slope of Ben Lomond Mountain. The Loma Prieta earthquake of 1989 and its aftershocks are recent reminders of the geologic unrest in the region.

California's broad system of strike-slip faulting has a long and complex history. Locally, the San Andreas, Zayante-Vergeles and San Gregorio faults and the Monterey Bay-Tularcitos fault zone present a seismic hazard to the subject project. These faults are associated with Holocene activity (movement in the last 11,000 years) and are therefore considered to be active. The most severe historical earthquakes to affect the project site are the 1906 San Francisco earthquake and the 1989 Loma Prieta earthquake, with Richter magnitudes of approximately 8.3 and 7.1, respectively.

9.3.1 Lithology

The lithology of the study area consists of Paleozoic, Mesozoic, Cretaceous, and Upper Miocene formations. The geologic units include three major lithologic groups: Mesozoic or Paleozoic metasedimentary rocks, Cretaceous igneous rocks, and an Upper Miocene sedimentary group (Brabb 1989). Sedimentary rocks (probably limestone and shale) of Permian age once formed the core of Ben Lomond Mountain. Before or during Cretaceous time (at least 65 million years ago) these rocks experienced folding, faulting and intrusion of igneous rocks (granodiorite, granite and related rocks), that metamorphosed the sedimentary rocks into marble and schist (Clark 1981).

During the subsequent geologic time periods (approximately 37 million years), these metamorphic rocks were folded further, uplifted, and then eroded. Sedimentary rocks including the Santa Margarita Sandstone of Miocene age were deposited on the eroded landscape (Clark 1981; Phillips 1990). Subsequent tectonic uplift of the coast range has further altered the landscape through canyon erosion, and erosional removal of the Santa Margarita Sandstone and other Tertiary formations from atop the marble body in some local areas. As a result of the complex geological processes, the sedimentary rocks make up the coastal terraces and canyon slopes to the south and form caps on some of the uplands to the north of the quarry (Wisser and Cox 1960). The metasedimentary rocks underlie the sedimentary sequence and are exposed in the quarry, hillsides, and canyons in the area.

The metasedimentary rocks are the oldest rocks exposed in the area. They are metamorphic rocks that include the marble that was being quarried at the Quarry and schist. The marble was originally deposited as limestone in a marine environment, and the schist represents fine-grained argillaceous sediments that were deposited at approximately the same time as the original limestone. The same intrusive events that metamorphosed the limestone to marble also changed the argillaceous materials to schist (Clark 1981). The marble is generally massive. Layered bedding is not readily apparent. The marble was most easily seen in the quarry area. Outcrops were also observed along local river valleys.

The schist is present over a large area to the northeast of the quarry and over a small area to the west of the quarry. Layers and lenses of schist are also present throughout the marble, as observed on the quarry walls. These schist stringers within the marble are most likely inter-bedded siltstone and mudstone within the original limestone, and they may help identify the orientation of the bedding in the marble. The overall dip of the inter-bedded schist units is to the southwest on the quarry walls, with a consistent strike to the northwest.

The Cretaceous igneous rocks are granitic rocks that have been described as granodiorite west and southwest of the quarry, and granite and adamellite northeast of the quarry (Brabb 1989). Intrusions of granitic rock are also evident in portions of the quarry walls. The intrusion of the igneous rocks provided the temperatures and pressures necessary for the metamorphosis to produce the marble and schist.

The igneous rocks form the basement rocks of the area, and the exposed marble and schist are the remnant pendants within or between the granite plutons.

Groundwater may occur within fractures in the granodiorite. Because the granodiorite appears to be producing only very limited quantities of water, it can act as a hydraulic barrier that confines most of the groundwater in the marble aquifer. The igneous rocks also help inhibit loss of water through deep flow.

The marble, schist, and granodiorite are overlain uncomfortably by the Upper Miocene Santa Margarita Sandstone, which consists of marine sandstone deposits. The Santa Margarita Sandstone has been described as thick-bedded to massive, fine to medium sand and thin-bedded conglomerates. It is gray to yellow, medium-grained, and generally well sorted in composition. It is friable to semi-consolidated. Its thickness is generally less than 50 feet but may be as much as 140 feet in some areas (Akers and Jackson 1977). The sandstone is overlain by minor outcrops of Santa Cruz Mudstone in portions of the area surrounding the quarry. This sandstone forms the erosional remnants on the tops of the nearby hills and northern uplands near the local resident communities. In addition to isolated sandstone outcrops surrounding the quarry, the sandstone also occurs south of the quarry near SP-1 Spring. Massive sandstone forms the lower slopes south of the quarry area. Further south of the quarry, the Santa Cruz Mudstone forms the high cliffs along the coast. These sedimentary formations strike northerly and dip gently to the west.

A significant landslide deposit exists in the immediate vicinity of SP-1 Spring. The spring itself appears to surface through the landslide deposits. This landslide area covers at least four to five acres. It includes debris from both the marble and Santa Margarita Sandstone. Intermittent seeps are present at the toe of the landslide. Significant shallow groundwater appears to be confined to the landslide deposits. Several seepage zones were identified in boreholes that were screened in the landslide deposit. Large-diameter boreholes at the toe of the slide indicated that groundwater does not appear to travel in significant quantities through the granitic bedrock, which acts as a boundary to water flow within the marble body. Monitoring data at several wells in the landslide deposit indicate that the water level increases, and conductivity decreases with precipitation events.

9.3.2 Geologic Structures

Geologic structure in the study area is a result of intrusion of granitic plutonic rocks at depth into metasedimentary country rock in Cretaceous time, followed by uplift and unroofing of the plutons and repeated cycles of sedimentary deposition and tectonic deformation throughout the Tertiary Period. Metamorphic rocks in the study area appear as a regularly bedded, but faulted, sequence of moderately to strongly metamorphosed sedimentary rock. The metamorphic rocks show a regular, approximate east–west strike with moderate northerly and southerly dips. However, bedded sections are discontinuous due to nearly ubiquitous faulting.

In areas with substantial marble, the metamorphic rocks are cut by orthogonal or near-orthogonal fractures, which are visible in the landscape as aligned valleys, swales, or notches in ridges. The fracture lineaments are often short and intersecting. In areas of karst, the fracture intersections are frequently marked by sinkholes. In some cases, these fractures are clearly faults with major displacement. In other cases, the fractures appear to have little displacement but have been etched into the landscape by preferential dissolution of the marble bedrock.

The marble, schist and granite rock in the quarry area have undergone extensive shearing and fracturing. The original bedding planes have been severely deformed and can hardly be recognized in the field. The quarry excavation reveals abundant fractures and joints at various orientations. The most common strike of the fractures is between N35°W and N50°W. These fractures dip vertically. They are often filled with clay.

Three faults were also inferred based on outcrop patterns before extensive excavation (Wisser and Cox 1960) and they are referred to as the north–south trending fault, the northwest-trending fault, and the northeast trending fault according to their orientations. The northeast-trending fault is coincident with the contact between the marble and schist. The northwest-trending fault is within the marble body. The fault oriented north south is roughly along the contact between the marble, schist and granodiorite and extends directly to SP-1 Spring. Aerial photographs also indicated a pronounced topographic lineament extending north-northwestwards from SP-1 Spring.

Figure 9.2 generally indicates that the surface topography and the paleo-bedrock elevation decrease from north to south. However, several large depressions are delineated based on the borehole data, and these depressions are within the marble body.

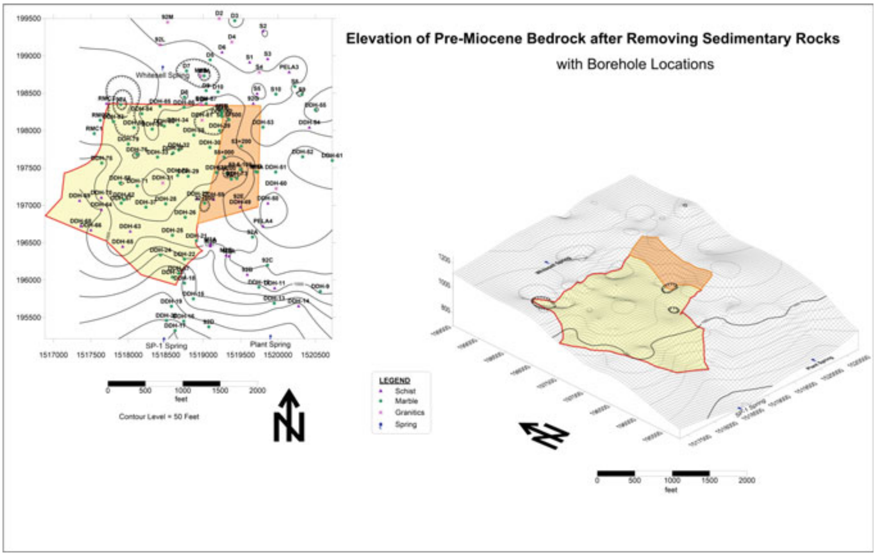

Fig. 9.2 Surface of pre-miocene bedrock

The most significant ones are along the contact between the marble and granitic rock to the north and northwest of the quarry. One is centered at M5A, and the other is centered at 92 J. These depressions appeared to be developed along fractures and joints.

Also evident is a valley trending from SP-1 Spring toward the north. This trend divides into two branches at the locations of DDH-23, DDH-67, and DDH-18. One trend continues in a northwest direction toward the depression centered at 92 J, and the other in a northeast direction, along which several depressions are aligned. These valleys are consistent with the inferred faults reported by Wisser and Cox (1960).

9.3.3 Karst and its Influence on Groundwater Flow

The study area has experienced episodes of subaerial erosion and submarine deposition throughout its geologic history, as indicated by the middle to upper Tertiary sedimentary sequence overlying the granitic and metamorphic basement. In the early to mid-Pleistocene, the study area was subject to sea level fluctuations of 300 to 400 feet every 100,000 years on average, caused by worldwide climatic variations and episodic glaciation in the higher latitudes. More recently, it has been elevated hundreds of feet above sea level and exposed to subaerial erosion for at least the last 500,000 years (mid Pleistocene to Holocene), based on estimated uplift rates for this section of the coastline. In other words, over the last 25 million years, the marble body in the study area has had an extraordinarily complex hydrogeologic history, characterized by dramatic fluctuations in climate and base level.

Groundwater flow in areas underlain by soluble rock, such as marble or limestone, is substantially different than groundwater flow in most other types of rock. In marble, the initial permeability may be quite low, but even slight downward flow over time will gradually dissolve the rock, forming solution channels through which water can flow more readily. In some cases, the solution channels enlarge to form caverns with underground ponds and streams. These solution cavities usually begin forming along bedding planes, fractures, or faults. In the quarry area, solution of the marble is strongly controlled by the fracture patterns. The influence of the fracture system on dissolution of marble bedrock and groundwater circulation is well documented by the alignment of sinkholes along major fractures (or faults) and particularly by the preferential location of prominent sinkholes (open or buried) at the intersection of two fractures.

The exposure afforded by the quarry walls provides a remarkable view of the hydrogeologic character of the marble over a vertical distance of 350 feet. Solution-widened fractures in the quarry walls are steeply dipping to vertical and commonly form continuous zones of solution channeling from the original ground surface through the quarry floor. The field reconnaissance of major karst features was conducted in accessible areas and the surface creeks. The main identified features included seven sinking streams, 31 springs, 27 sinkholes, and seven caves. The features relevant to the tracer tests are shown in Fig. 9.3.

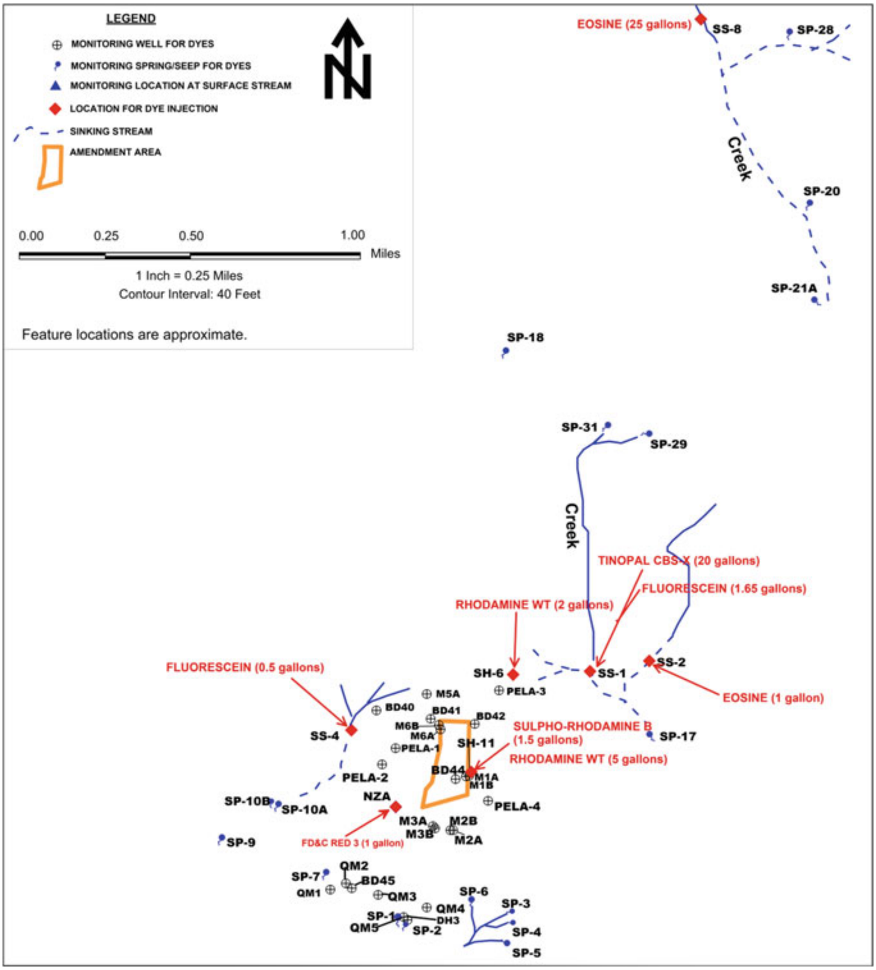

Fig. 9.3 Dye tracer injection and monitoring locations

9.4 Source Investigation for SP-1 Spring with Dye Tracing

The groundwater tracing was conducted to determine the water sources for SP-1 Spring and the preferential flow paths to the spring by introducing fluorescent dyes into sinking streams, sinkholes, and boreholes and monitoring their discharge at springs, seeps, streams, and wells. Information from this investigation has been critical in understanding the karst system at the site. It is also applicable to evaluating the potential impact of quarry operations on SP-1 Spring. The generalized capture zone for SP-1 Spring has been determined by combining the results from the tracing tests and other information related to the hydrogeology of the site. The delineation of the catchment basin for SP-1 Spring provides the information necessary to assist with the mitigation of the episodic turbidity problem at the spring. Groundwater-tracing data are also used to make recommendations for future quarrying operations to avoid adverse impacts on SP-1 Spring.

9.4.1 Previous Groundwater Tracing at Study Site

Five groundwater tracing tests had been conducted in the area prior to the current investigation. The details of each tracer test are summarized in the following section.

9.4.1.1 Tracer Test in DDH-33

On March 12, 1959, the first sugar tracer test was conducted in a diamond drill hole in the quarry area—DDH-33 (Wisser and Cox 1960). The linear distance between SP-1 Spring and DDH-33 is approximately 2450 feet. Groundwater elevation in this hole was reported at 768 feet amsl at the time of the tracing test. Five hundred pounds of sugar (300 gallons of sugar syrup in the concentration of 200,000 parts per million (ppm) were injected into DDH-33. SP-1 Spring and SP-3 Spring were monitored for sugar syrup for 14 days, and no sugar was detected at either of the monitored springs.

9.4.1.2 Tracer Test in DDH-26

On March 20, 1959, a second sugar tracer test was conducted in a diamond drill hole in the quarry area—DDH-26 (Wisser and Cox 1960). The linear distance between SP-1 Spring and DDH-26 is approximately 1670 feet. Groundwater elevation in this hole was reported at 810 feet amsl at the time of the tracing test. One thousand pounds of sugar (300 gallons of sugar syrup in the concentration of 400,000 ppm) were injected into DDH-26. Both SP-1 Spring and SP-3 Spring were monitored for sugar syrup for 14 days, and no sugar was detected at either of the monitored springs.

9.4.1.3 Tracer Test in SH-2

On May 13, 1959, a third tracer test was conducted in a sinkhole within SS-4 (most likely sinkhole SH-2) (Wisser and Cox 1960), which is located northwest of the quarry. Five hundred pounds of sugar (300 gallons of sugar syrup in the concentration of 200,000 ppm) were injected into the sinkhole. Both SP-1 Spring and SP-3 Spring were monitored for 82 h, and no sugar was detected at either of the monitored springs.

9.4.1.4 Tracer Test in DDH-19

On August 5, 1964, a fourth sugar tracer test was conducted in a diamond drill hole—DDH-19. DDH-19 is located approximately 450 feet north of SP-1 Spring. One thousand pounds of sugar (three hundred gallons of sugar syrup in the concentration of 400,000 ppm) were injected into this borehole. Only SP-1 Spring was monitored during the test. Sugar was first detected at SP-1 Spring 6.5 days after the sugar introduction and was consistently detected for a period of at least 26 days. The breakthrough curve at SP-1 Spring is very sporadic and does not represent a typical breakthrough curve. The highest concentration of sugar (10 ppm) occurred after a water sample at the injection borehole was collected and analyzed for the injected sugar.

9.4.1.5 Tracer Test in Surface Creek

A fifth tracer test was conducted in 1998 using bromide. The bromide tracer (amount unknown) was introduced into a sinkhole along a local Creek, which is most likely located at SS-1. This sinkhole was not observed in the present study, and it was likely filled up by river deposits. The total flow into the sinkhole was visually estimated at 75 to 150 gpm at the time of tracer injection. Both SP-1 Spring and SP-3 Spring were monitored over a period of 24 to 36 h, and no bromide was detected at either of the monitored springs.

9.4.2 Selection of Tracers

All chosen tracer substances should exhibit certain characteristics, and the selected tracers should not:

- Change the hydraulic characteristics of the traced water.
- Cause contamination of the water of the springs including SP-1 Spring beyond permissible standards.
- Lead to the emergence of toxic by-products following physical, chemical, or biological degradation.
- Affect tastes, odor, or color of the water at SP-1 Spring.

Other factors that were considered in selecting the tracers include conservative behavior, solubility in water, and ease of detection at low concentrations. Based on these criteria, fluorescent dyes were selected in the tracing study. Fluorescent dyes have been used as effective groundwater tracers for over 200 years, and they have been employed in most karst sites in the United States (U.S.) (Environmental Protection Agency [EPA] 1996). Fluorescent dyes are often the first choice to label groundwater for tracing studies in karst aquifers (Quinlan 1986). They are very soluble in water and can be detected at very low concentrations. Several of the dyes are sold under Drug and Cosmetic (D&C) names because they are used in such products. The fluorescent dyes are National Sanitation Foundation (NSF) certified for use in drinking water and they are often used to inspect water heating, cooling and processing systems for leaks.

There is extensive technical literature (Field et al. 1995; Smart and Laidlaw 1977; Smart 1984) demonstrating that fluorescent dyes present no health or environmental problems at concentrations five orders of magnitude or more above the method detection limit of modern protocols. A detailed discussion of the effects of the commonly used dyes on warm-blooded animals, fish and other water organisms, plants, and microorganisms is provided by Käss (1998). Based on the U.S. EPA approved methods, Field et al. (1995) concluded that none of the commonly used dyes presents a significant health or environmental problem if the dye concentrations are maintained below 1–2 mg/l for 24 h at the point of groundwater withdrawal or discharges.

Nonetheless, the commonly used fluorescent dyes have their maximum fluorescence in the visible wavelength range from 380 to 760 nm (nm). The psychological adversities that can occur due to a visible reemergence of dyes from SP-1 Spring were avoided in this study. The U. S. Geological Survey recommends that during tracing tests, the highest concentration of fluorescent dyes at the observation sites should be under 10 μg/l (Mull et al. 1988; Hubbard et al. 1982), which is far below the visible limit, to avoid such an aesthetic effect. In implementing the proposed tracer tests, the USGS guidelines were followed to minimize conspicuous coloration of the spring waters. Every effort was made to keep the concentrations of the fluorescent dyes less than 10 μg/l at SP-1 Spring while having a successful groundwater trace.

Six fluorescent dyes were used in this investigation, and their properties are listed in Table 9.1. The background conditions of these fluorescent dyes were tested at most of the monitoring locations prior to dye introduction. Although several of the dyes were detected at various locations, their concentrations are not unusually high and do not indicate that the water in the area was contaminated by any of the selected dyes.

9.4.3 Dye Injection

The dye injection was conducted in four separate phases with four dyes injected in the first phase, two dyes injected in the second phase, two dyes injected in the third phase, and one dye injected in the fourth phase. The initial dye tracing work plan included the first two phases. The third phase was added to the investigation based on the results from the first two phases. The fourth phase was added to the investigation because a new sinking stream was identified during low flow conditions. Within each phase involving more than one dye, the dyes were injected in a sequential manner to minimize their impacts on SP-1 Spring in case waters at more than one location have hydraulic connections to SP-1 Spring. This strategy would also help identify the presence of a particular dye in the dye analysis instrument spectrofluorophotometer.

Table 9.1 Selected fluorescent tracer dyes and their properties

Dye (Alternate name)	Color index name	Color index number	Chemical abstract service (CAS) number	Emission wavelengths[1] (nm)		Fluorescence intensity (%)	Adsorption tendency
				Eluted sample	Water sample		
Eosine (Eosine OJ, D&C Red 22)	Acid red 87	45,380	17,372–87–1	542	535	18	Low
Fluorescein (Uranine, Uranine C, Sodium Fluorescein, Fluorescein LT, Fluorescent Yellow/Green, D&C Yellow 8)	Acid yellow 73	45,350	518–47–8	516.5	508	100	Very low
Rhodamine WT (Fluorescent Red, Red Fluorescent Dye)	Acid red 388	None assigned	37,299–86–8	568.5	576	25	Moderate
Sulphorhodamine B (Sulfo Rhodamine B, Pontacyl Brilliant Pink B, Lissamine Red 4B, Kiton Rhodamine B, Acid Rhodamine B, Amido Rhodamine B, Fluoro Brilliant Pink)	Acid red 52	45,100	3520–42–1	576.5	582	30	Moderate
Tinopal CBS-X (Optical Brightener)	Fluorescent brighter 351		54,351–85–8	398	397	60	Moderate
FD&C Red #3	Food red 14	45,430	16,423–68–0	549	555	?	?

Sources (EPA 2002; Aley 1999; Crawford Hydrology Lab 2003)
?, No data available
1. Values are approximate only. Different instruments may yield slightly different results

The following sections discuss the locations and procedures for introducing the fluorescent dyes to trace the groundwater flow in the marble aquifer.

9.4.3.1 Locations for Dye Injection and Mass of Dye

The locations for the dye injection and the type of dye that was introduced at each location are shown in Fig. 9.3. Table 9.2 provides detailed information including the mass of dye that was used at each location. One monitoring well, two sinkholes, and four sinking streams were used for the dye injection. The same locations were used for the dye injection in the second and third phases. The fluorescent dyes used in this investigation are in liquid form, and their strengths (mass of dye [kg] per gallon of mixture) are also given in Table 9.2.

Determination of the necessary tracer mass is one of the most difficult aspects to estimate for a proposed tracer test (Field 2002). Although many estimation equations have been developed over the last century primarily for karstic terranes, the tracer mass released in most tracer studies is typically a guess utilizing the experience of the investigator (Alexander and Quinlan 1992). This is because each karst setting is unique, and a simple algebraic expression that appears to function adequately in one setting is not necessarily applicable to other settings. The equations are only useful to provide some general guidelines as to the amount of dyes to be used. Of these equations, three are particularly useful, as suggested by Worthington and

Table 9.2 Sequence of dye injection

Phase	Dye type	Location	Volume of dye mixture (gallon)	Mass of dye (kg)/Gallon mixture	Amount (kg)
I	FD&C Red 3	Borehole NZA	1.0	0.39462	0.39
	Fluorescein	Sink stream, SS-4	0.5	1.87	0.935
	Eosine	Sinking stream, SS-2	1.0	0.964	0.964
	Rhodamine WT	Sinkhole, SH-6	2.0	0.794	1.588
II	Sulphorhodamine B	Sinkhole, SH-11	1.5	0.20412	0.31
	Tinopal CBS-X	Sinking stream, SS-1	20.0	0.17962	3.59
III	Rhodamine WT	Sinkhole, SH-11	5	0.794	3.97
	Fluorescein	Sinking stream, SS-1	1.65	1.89	3.12
IV	Eosine	Sinking stream, SS-8	25	0.964	24.1

Smart (2003). These equations suggest that the amount of dye to be injected is closely related to the distance or travel time to the monitoring location, the discharge and the target dye concentration at the monitoring location. They were used for a rough estimation in this tracer design, and the amount of dyes estimated from these equations was modified based on the conditions of the specific site (sinking stream, sinkhole or borehole), estimated flow rate (if there is flow), type of overburden, type of dye, distance to SP-1 Spring, estimated discharge at SP-1 Spring, the maximum concentration to be detected at SP-1 Spring, and investigator's experience in similar settings.

The uncertainty of the dye adsorption by earth materials, the lack of adequate understanding of the groundwater flow (an answer to be obtained through dye tracing), dilution, dispersion and diffusion processes, and the vagaries of the weather (whether any rain is expected during the course of the tests) further complicate the accurate estimation of the mass of dye to be used. A safety factor is included in the mass estimation to account for the uncertainties of various factors and the complexities of the hydrogeological settings. Dye tracing may have to be repeated if a negative detection of dye is possibly caused by injection of an insufficient mass of dye.

9.4.3.2 Tracer Injection at Sinking Streams

Injection of fluorescent dyes into sinking streams is relatively simple. At SS-4, fluorescein dye was poured into the creek approximately 50 feet upstream from the main sinking point. The flow rate was approximately 5 gallons per minute (gpm). Several small dead-end side channels retained a small portion of the dye. The majority of the dye flowed with the water and sank into the subsurface. A swallow hole was visible at the bottom of the sinkhole and took most of the water into the subsurface. The dye injection lasted approximately 10 min.

Eosine dye was used at SS-2. The surface water gradually sank into the subsurface as it flowed through the marble section. No distinct sinking point was observed. The flow rate was approximately 80 gpm at the time of the dye injection. Eosine was poured approximately 20 feet upstream from the point where the valley was dry. The dye injection lasted approximately 8 min.

When Tinopal CBS-X was introduced at SS-1, a significant portion of the surface water was continuing to flow downstream of the marble section in the creek. The total flow was estimated to be approximately 700 gpm 50 feet upstream. The flow rate was approximately 300 gpm approximately 200 feet downstream. Two distinctive sinking points were observed at the time of injection and both are located on the western bank of the river at elevations that are a couple of inches higher than the riverbed. The major sinking point appears to be a cave entrance one foot in diameter. This small cave took approximately 50 gpm of water into the subsurface. It is conceivable that more water can flow into the cave when the water level in the creek is higher. Another sinking point is 10 feet south from the small cave. At least 10 gpm of water sank into the surface through the sand overburden. The continuous water flow into the subsurface at this location resulted in a small depression in the sand. Because of the flow conditions in the creek, Tinopal CBS-X was introduced into three different locations: 10 gallons of dye at the small cave entrance, 2.5 gallons of dye at the sinking point through sandy overburden, and 7.5 gallons of dye at the main stream. The total injection duration was 10 min.

The tracing was repeated during a low-flow condition when all the water in this creek sank underground at SS-1. The amount of 1.65 gallons of fluorescein dye was poured into the creek at the cave entrance just below the abandoned dam. The flow was estimated to be 15 gpm. No dye was visible beyond the sinking point in the creek.

Tracing at SS-8 took place after it was identified as a sinking stream during the low-flow condition. Twenty-five gallons of Eosine was poured at the waterfall 150 feet upstream from the sinking point. The total length of the sinking section was approximately 200 feet. The total stream flow, estimated approximately at 240 gpm, was lost over this section.

9.4.3.3 Tracer Injection at Sinkholes

Tracer injection at sinkholes is more complicated than that in sinking streams. Injection of the dyes into the sinkholes was facilitated by injection of water using a water truck. A swallow hole was visible at the bottom of sinkhole SH-6. Prior to the dye injection, approximately 2,500 gallons of water were used to pre-wet the sinkhole and the underground passages. Then two gallons of Rhodamine WT were injected at the bottom of the sinkhole in 5 min. The "primer" water was introduced into the sinkhole at a rate of approximately 50 gpm. The injected water and dye were pushed into the subsurface very quickly. An open channel was visible at the bottom of the sinkhole. After the dye injection, approximately 6,500 gallons of water were used to "chase" the dye and facilitate the injection process. The "chaser" water was injected into the sinkhole at a rate of approximately 100 gpm.

Sinkhole SH-11 was a backfilled sinkhole. In order to introduce the dye into this sinkhole, it was reopened by removing several tons of rock fragments and soil. The excavation stopped when a large void was exposed, and preliminary permeability tests indicated that the void could take at least 50 gpm of water. The void was formed between rock fragments, and it was not within the marble body. Similar to the injection process at SH-6, 2000 gallons of water were used to pre-wet the sinkhole and the underground passages; moreover, 4500 gallons of water were introduced one day earlier for the permeability test. One and a half pounds of Sulphorhodamine B was injected into this location in 5 min. After the dye injection, 7000 gallons of water were used to chase the dye and facilitate the injection process. The objective of using the chaser water is to prevent the tracer dye from getting stored in large dead-end voids and behind other obstructions.

The tracing at SH-11 was repeated using a different tracer in a larger quantity. After the sinkhole was reopened again, 3000 gallons of water were used to pre-wet the system. While the water continued to flow into the sinkhole, five gallons of

Rhodamine WT were injected. Immediately after the dye injection, 4000 gallons of water were used to chase the injected dye.

9.4.3.4 Tracer Injection at Monitoring Well NZA

Both primer and chaser water were used in tracer injection at the monitoring well NZA. NZA was drilled into the marble at the bottom of the quarry. The water injection rate was very small (<5 gpm) to avoid an excessive increase of the water level in the well. An excessive increase of the water level would create an unnatural condition. The water level was also monitored prior to the dye injection to ensure that the primer water had already moved into the aquifer. Two pounds of Red #3 were injected into the borehole via a garden hose. After the dye injection, a small amount of water was used to help push the dye into the aquifer. The total amount of water used to chase the dye was no more than 500 gallons.

9.4.4 Dye Monitoring

The main objective of the proposed groundwater tracing tests was to investigate the recharge sources for SP-1 Spring. However, SP-1 Spring was not the only location for dye monitoring in this study. An attempt was made to obtain as much information as possible to better understand the hydrogeological conditions in the quarry area, especially the flow paths to SP-1 Spring or SP-3 Spring. Therefore, the monitoring locations for the tracer tests included springs, monitoring wells, and locations at local creeks that are located downstream of the dye injection points. The monitoring effort is different at each location, depending upon its hydrogeological significance to the study.

9.4.4.1 Monitoring Locations

The monitoring locations were selected based on the results from the karst inventory and their elevations in relation to SP-1 Spring and the dye injection points. Table 9.3 lists the locations that were monitored during the tracer study. Forty-nine locations were identified for dye monitoring, including ten locations at local creeks, 13 springs (SP-1 through SP-10, SP-18, and SP-28), 25 monitoring wells, and one at the water tank in the quarry. The characteristics of the springs and creeks have been discussed in the karst inventory section. During the dye tracing, a request was made not use the water at the springs.

Table 9.3 Monitoring for fluorescent dyes

Monitoring Locations		Phases	Sampling effort
Springs/Seeps	SP-1	I, II, III, IV	The dye bugs were retrieved and replaced on a weekly basis. An automatic sampler was used to collect water samples. The sampling frequency varied from 30 min to 36 h, depending on the breakthrough process. Sampling frequency was much higher immediately after each dye injection
	SP-2	I, II	The dye bugs were retrieved and replaced on a weekly basis. The water samples were collected at the same time when their dye bugs were replaced
	SP-3	I, II, III, IV	The dye bugs were retrieved and replaced on a weekly basis. An automatic sampler was used to collect water samples. The sampling frequency varied from 1 to 48 h, depending on the dye breakthrough process. Sampling frequency was much higher immediately after each dye injection
	SP-4	I, II	The dye bugs were retrieved and replaced on a weekly basis. The water samples were collected at the same time when their dye bugs were replaced. Additional water samples were collected every 4 h for the first 10 days and then changed to daily until the end of their monitoring
	SP-5	I, II	The dye bugs were retrieved and replaced on a weekly basis. The water samples were collected at the same time when their dye bugs were replaced. Additional water samples were collected every 4 h for the first 10 days and then changed to daily until the end of their monitoring
	SP-6	I, II	The dye bugs were retrieved and replaced on a weekly basis. The water samples were collected at the same time when their dye bugs were replaced. Additional water samples were collected every 4 h for the first 10 days and then changed to daily until the end of their monitoring
	SP-7	I, II	The dye bugs were retrieved and replaced on a weekly basis. The water samples were collected at the same time when their dye bugs were replaced. Additional water samples were collected every 4 h for the first 10 days and then changed to daily until the end of their monitoring
	SP-8	I, II	The dye bugs were retrieved and replaced on a weekly basis. The water samples were collected at the same time when their dye bugs were replaced. Additional water samples were collected every 4 h for the first 10 days and then changed to daily until the end of their monitoring
	SP-9	I, II	The dye bugs were retrieved and replaced on a weekly basis. The water samples were collected at the same time when their dye bugs were replaced. Additional water samples were collected every 4 h for the first 10 days and then changed to daily until the end of their monitoring

(continued)

Table 9.3 (continued)

Monitoring Locations		Phases	Sampling effort
	SP-10A	I, II	The dye bugs were retrieved and replaced on a weekly basis. The water samples were collected at the same time when their dye bugs were replaced. Additional water samples were collected every 4 h for the first 10 days and then changed to daily until the end of their monitoring
	SP-10B	I, II	The dye bugs were retrieved and replaced on a weekly basis. The water samples were collected at the same time when their dye bugs were replaced. Additional water samples were collected every 4 h for the first 10 days and then changed to daily until the end of their monitoring
	SP-17	I, II	The dye bugs were retrieved and replaced on a weekly basis. The water samples were collected at the same time when their dye bugs were replaced
	SP-21	IV	The dye bugs were retrieved and replaced on a weekly basis. An automatic sampler was used collect water samplers at the confluence of the flows from SP-21 and SP-30. The sampling frequency varied from 24 to 48 h. After the automatic sampler was removed on December 8, 2004, the water samples were collected at the same time when their dye bugs were replaced
	SP-28	IV	The dye bugs were retrieved and replaced on a weekly basis. The water samples were collected at the same time when their dye bugs were replaced
	SP-29	IV	The dye bugs were retrieved and replaced on a weekly basis. The water samples were collected at the same time when their dye bugs were replaced
	SP-30	IV	The dye bugs were retrieved and replaced on a weekly basis. An automatic sampler was used collect water samplers at the confluence of the flows from SP-21 and SP-30. The sampling frequency varied from 24 to 48 h. After the automatic sampler was removed on December 8, 2004, the water samples were collected at the same time when their dye bugs were replaced
	SP-31	IV	The dye bugs were retrieved and replaced on a weekly basis. The water samples were collected at the same time when their dye bugs were replaced
	SP-18	IV	The dye bugs were retrieved and replaced on a weekly basis. The water samples were collected at the same time when their dye bugs were replaced
Creeks	SS-1	I, II, IV	The dye bugs were retrieved and replaced on a weekly basis. The water samples were collected at the same time when their dye bugs were replaced
	CR-2	I, II, IV	The dye bugs were retrieved and replaced on a weekly basis. The water samples were collected at the same time when their dye bugs were replaced

(continued)

Table 9.3 (continued)

Monitoring Locations		Phases	Sampling effort
	CR-4	I, II, IV	The dye bugs were retrieved and replaced on a weekly basis. The water samples were collected at the same time when their dye bugs were replaced
	CR-5	I, II	The dye bugs were retrieved and replaced on a weekly basis. The water samples were collected at the same time when their dye bugs were replaced
	CR-6	IV	The dye bugs were retrieved and replaced on a weekly basis. The water samples were collected at the same time when their dye bugs were replaced
Wells	QM-1	I, II	The dye bugs were retrieved and replaced on a weekly basis. The water samples were collected at the same time when their dye bugs were replaced
	QM-2	I, II	The dye bugs were retrieved and replaced on a weekly basis. The water samples were collected at the same time when their dye bugs were replaced
	QM-3	I, II	The dye bugs were retrieved and replaced on a weekly basis. The water samples were collected at the same time when their dye bugs were replaced
	QM-4	I, II	The dye bugs were retrieved and replaced on a weekly basis. The water samples were collected at the same time when their dye bugs were replaced
	QM-5	I, II	The dye bugs were retrieved and replaced on a weekly basis. The water samples were collected at the same time when their dye bugs were replaced
	M1A	I, II	The dye bugs were retrieved and replaced on a weekly basis. The water samples were collected at the same time when their dye bugs were replaced
	M1B	I, II, III, IV	The dye bugs were retrieved and replaced on a weekly basis. The water samples were collected at the same time when their dye bugs were replaced. In the third and fourth phases' dye tracing, water samples were collected daily
	M2A	I, II	The dye bugs were retrieved and replaced on a weekly basis. The water samples were collected at the same time when their dye bugs were replaced
	M2B	I, II	The dye bugs were retrieved and replaced on a weekly basis. The water samples were collected at the same time when their dye bugs were replaced
	M3A	I, II	The dye bugs were retrieved and replaced on a weekly basis. The water samples were collected at the same time when their dye bugs were replaced
	M3B	I, II	The dye bugs were retrieved and replaced on a weekly basis. The water samples were collected at the same time when their dye bugs were replaced

(continued)

Table 9.3 (continued)

Monitoring Locations		Phases	Sampling effort
	M5A	I, II, III, IV	The dye bugs were retrieved and replaced on a weekly basis. The water samples were collected at the same time when their dye bugs were replaced. In the third and fourth phases' dye tracing, water samples were collected daily
	M6A	I, II	The dye bugs were retrieved and replaced on a weekly basis. The water samples were collected at the same time when their dye bugs were replaced
	M6B	I, II	The dye bugs were retrieved and replaced on a weekly basis. The water samples were collected at the same time when their dye bugs were replaced
	BD-40	I, II	The dye bugs were retrieved and replaced on a weekly basis. The water samples were collected at the same time when their dye bugs were replaced
	BD-41	I, II	The dye bugs were retrieved and replaced on a weekly basis. The water samples were collected at the same time when their dye bugs were replaced
	BD-42	I, II	The dye bugs were retrieved and replaced on a weekly basis. The water samples were collected at the same time when their dye bugs were replaced
	BD-44	I, II	The dye bugs were retrieved and replaced on a weekly basis. The water samples were collected at the same time when their dye bugs were replaced
	BD-45	I, II	The dye bugs were retrieved and replaced on a weekly basis. The water samples were collected at the same time when their dye bugs were replaced
	DH-3	I, II	The dye bugs were retrieved and replaced on a weekly basis. The water samples were collected at the same time when their dye bugs were replaced
	NZA	I, II, III, IV	The dye bugs were retrieved and replaced on a weekly basis. The water samples were collected at the same time when their dye bugs were replaced. In the third and fourth phases' dye tracing, water samples were collected daily
	PELA-1	I, II	The dye bugs were retrieved and replaced on a weekly basis. The water samples were collected at the same time when their dye bugs were replaced
	PELA-2	I, II	The dye bugs were retrieved and replaced on a weekly basis. The water samples were collected at the same time when their dye bugs were replaced
	PELA-3	I, II	The dye bugs were retrieved and replaced on a weekly basis. The water samples were collected at the same time when their dye bugs were replaced
	PELA-4	I, II	The dye bugs were retrieved and replaced on a weekly basis. The water samples were collected at the same time when their dye bugs were replaced

(continued)

Table 9.3 (continued)

Monitoring Locations	Phases	Sampling effort
Water tank	I, II	The dye bugs were retrieved and replaced on a weekly basis. The water samples were collected at the same time when their dye bugs were replaced

9.4.4.2 Sampling Methods and Sampling Frequencies

Two different samples were collected at each location for dye analysis—grab samples of water and activated charcoal samples (dye receptors or "dye bugs"). The use of both sampling methods was to minimize the risk of misinterpretations and maximize the detection of any low concentrations of the dyes.

Water Samples

Grab samples were collected using 30 ml glass vials. Water samples at the creeks and springs were collected directly. At the springs, the sampling locations were chosen to be as close to the spring orifice as possible. At monitoring wells, the water samples were collected using disposable bailers. The sampling frequency was weekly at the monitoring wells. Two automatic water samplers were stationed at SP-1 Spring and SP-3 Spring to collect the water samples. A filter fluorometer was used to analyze the concentration of Fluorescein, Rhodamine WT, and Eosine to help select the water samples to be sent for laboratory analysis.

Dye Receptors

Packets of activated charcoal (commonly called dye bugs) were used in all the monitoring locations. The use of activated charcoal helps assure dye detection because the low dye concentrations found in water samples may not be measurable or sampling frequencies may not have been adequate. The ability of activated charcoal to continuously adsorb and concentrate fluorescent dyes provides a sound means for determining the occurrence of the fluorescent dyes but not a quantitative value of the concentration of the dye.

Two sets of dye bugs were placed at the springs and creeks to account for the possible loss of the bugs during their one-week deployment. The dye bugs at the springs and creeks were placed in such a way that the maximum amount of water would pass through them. The dye bugs in the monitoring wells were placed within their screen intervals. The dye concentration measured in the dye-eluant mixture cannot be related directly to its concentration in the water sample. However, bugs can accumulate and magnify low concentrations of dye passing through them over an extended period, thus effectively lowering the limit of detection.

Sampling Frequencies and Monitoring Duration

The dye bugs were retrieved and replaced on a weekly basis. The frequency of water sample collection was evaluated for each individual monitoring station, and the frequency varied as the groundwater flow system became more understood. Table 9.3 lists the sampling frequency and monitoring duration for each location.

9.4.5 Dye Analyses and Results

Collected dye receptors and selected water samples were analyzed analysis using a Shimazu RF-5301 PC Synchronous Scanning Spectrofluorophotometer. For the six dyes used in this study, a synchronous scan is performed where the excitation and emission monochromators are kept at a fixed wavelength separation during the scan. If the scan indicates positive results for the dyes, the concentration of the dye is then calculated based on the calibrations curves stored in the instrument or computer. If the emission spectra from two or more dyes overlay, then the spectra for each dye are separated by use of a non-linear curve-fitting computer software specifically designed for spectral separation (Crawford Hydrology Lab 2003).

Because both water samples and dye receptors were used for dye analysis, a positive detection is defined when either a typical dye breakthrough was established or when the tracer-dye concentration in two consecutive dye receptors exceeded ten times the background concentration at the same location, as recommended by Crawford Hydrology Lab (2003). If the background value is not detectable, then the quantitation limit for the dye was used for the background value (Table 9.4). Using ten times the background concentration ensures that the detection of the dye is positive, but it may also increase the false negative rate. Therefore, one more category was defined in this project—a likely positive detection. The likely positive detection was defined when the tracer-concentration in two consecutive dye receptors exceeded its background value by five times but less than ten times or when the breakthrough curve of a dye was not well defined due to low concentration of the dye.

Table 9.4 Quantitation limit of fluorescent dyes

Dyes	Quantitation limits (ug/l)	
	Dye receptor	Water sample
Eosine	0.005	0.01
Fluorescein	0.005	0.01
Rhodamine WT	0.005	0.01
Sulphorhodamine B	0.005	0.01
Tinopal CBS-X	0.1	0.1
FD&C Red 3	0.05	0.1

According to the criteria set above for positive detection, all four injected dyes in the first phase of tracing—Eosine, Fluorescein, Rhodamine WT and Red 3, were detected at SP-1 Spring or SP-3 Spring. Four monitoring wells—M1B, M5A, NZA, and QM5 had positive detections of at least one of the dyes. No dye was positively detected in other springs/seeps other than SP-1 Spring and SP-3 Spring.

The two dyes, Sulphorhodamine B injected at SH-11 and Tinopal CBS-X injected into sinking stream SS-1 during the second phase had not been detected at the monitoring station over the monitoring period. Tinopal CBS-X was detected at SP-17, which is in the same creek as SS-1 and downstream of the dye injection point. Because a portion of the water in the creek flowed to SP-17, this detection was not conclusive.

Of the two dyes injected in the third phase, the Fluorescein injected at SS-1 was detected at SP-1 Spring and SP-3 Spring. Two monitoring wells—M1B and M5A also had positive detection of the Fluorescein. The Rhodamine WT injected in SH-11 in the third phase, however, has not been detected at any monitoring stations.

The Eosine injected in SS-8 in the fourth phase was positively detected at SP-1 Spring and SP-3 Spring. The Eosine was also detected at springs SP-21 and SP-30 and monitoring well M1B.

The results of the groundwater tracing investigation are summarized in Table 9.5. The generalized routes of subsurface flow are depicted in Fig. 9.4.

9.4.5.1 Connection from Monitoring Well NZA to SP-1 Spring

Water at monitoring well NZA has a strong connection to SP-1 Spring. The Red 3 dye that was injected at NZA was detected in the water sample at SP-1 Spring 7 h after the dye injection, and its concentration reached a peak within 7.5 h, as shown in Fig. 9.5. After its peak, the concentration decreased quickly. The breakthrough curve is typical for karst aquifers and indicative of conduit flow in the marble aquifer beneath the quarry bottom. Well logs in NZA also show that this well intercepts a fracture system. The map distance between NZA and SP-1 Spring is approximately 800 feet. The groundwater flow rate based on the first arrival of the dye was estimated to be 110 feet/h, or 2,760 feet/day. Because of the tortuous flow path and the elevation difference between these two locations, this estimated water flow rate might represent the minimum flow rate. However, the dispersion process of the dye in the groundwater system further complicates the flow rate calculation. If the time to reach the peak concentration of the dye was used, the flow rate was approximately 107 feet/h, or 2,560 feet/day.

Although the dye concentration in water samples at SP-1 Spring decreased very quickly, the concentrations of Red 3 in the dye receptors were positively detected until June 25, 2004. Figure 9.6 shows the Red 3 concentrations in the dye receptors at SP-1 Spring. The dye receptors for the first two weeks had the most concentrated dye. It appears that a portion of the Red 3 was pushed into the aquifer system, but a significant amount of dye was retained in the well. The concentrations of Red 3

Table 9.5 Summary of dye tracing results

Phases	Monitoring locations	Tracer Insertion						
		Monitoring well, NZA	Sinking stream, SS-4	Sinking stream, SS-2	Sinkhole, SH-6	Sinkhole, SH-11	Sinking stream, SS-1	Sinking stream, SS-8
Phases I and II	SP-1	+7 h (1)	+66 days (2)	+ ? 29 days (1)	+3.3 day (1)	–	–	
	SP-3	–	–	+5.9 days (1)	–	–	–	
	SP-17	–	–	–	–	–	+7 days (2)	
	QM-5	+11 days (2)	–	–	–	–	–	
	M1B	–	–	+38 days (2)	–	–	–	
	M5A	–	–	–	+ ?	–	–	
	NZA	Injection point	+45 days (2)	–	+45 days (2)	–	–	
Phases III and IV	SP-1					–	+13 days (2)	+67 days (2)
	SP-3					–	+6 days (2)	+67 days (2)
	SP-21					–	–	+29 days (2)
	SP-30					–	–	+29 days (2)
	CR-2					–	–	+37 days (2)
	M1B					–	+21 days (2)	+37 days (2)
	M5A					–	+126 days (2)	–

\+ Positive detection
\+ ? Likely positive detection
– Negative detection
(1) The time is from dye insertion to first detection of the dye based on water samples
(2) The time is from dye insertion to first detection of the dye based on dye receptors

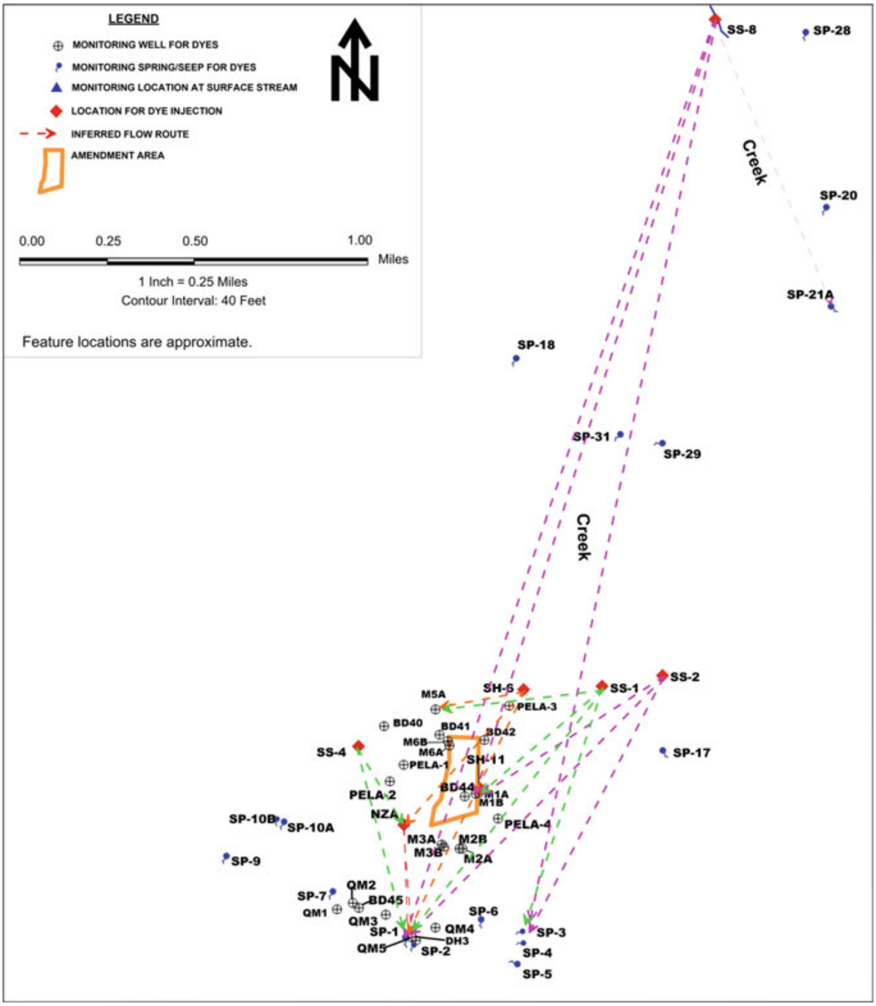

Fig. 9.4 Generalized groundwater flow routes based on tracer test results

in the dye receptors were still very high in NZA until the end of the monitoring of Red 3.

9.4.5.2 Connection from Monitoring Well NZA to Monitoring Well QM5

Red 3 was positively detected at QM5 in the dye receptors that were collected the second and third weeks after the dye injection. The dye concentration peaked 20 days after the dye injection. The concentrations are not as high at those at SP-1 Spring.

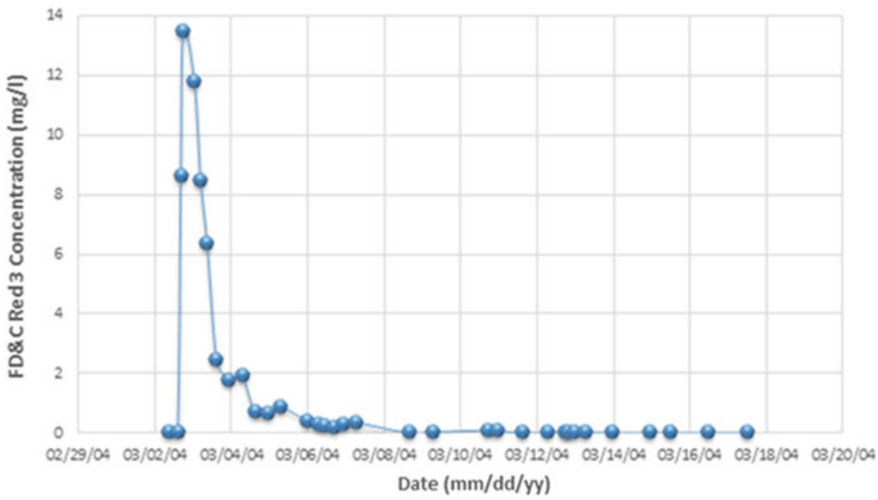

Fig. 9.5 Fluorescent dye red 3 breakthrough curve for water samples at SP-1 spring

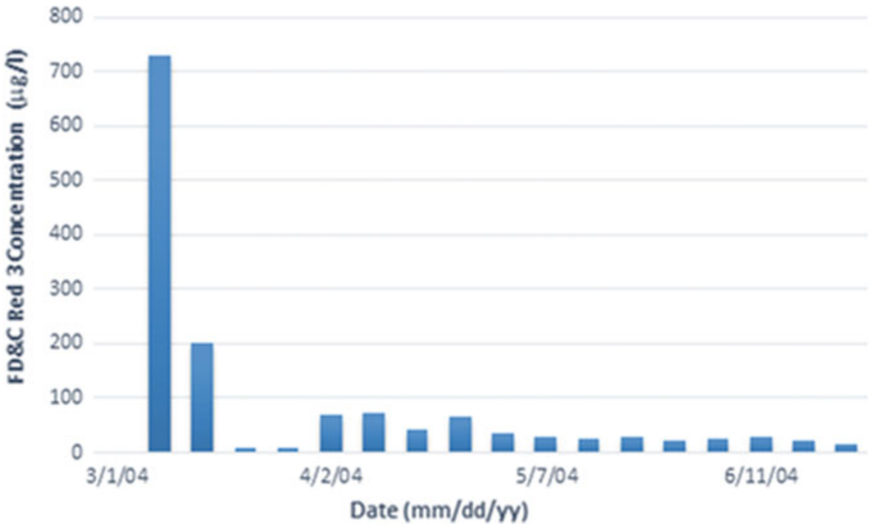

Fig. 9.6 Fluorescent dye red 3 laboratory results for dye receptors at SP-1 spring

QM5 is adjacent to SP-1 Spring but screened in the landslide deposits. It is unlikely that the Red 3-tagged water at NZA can flow to QM5 through a separate flow path that is different from that to SP-1 Spring. It is likely that the water at SP-1 Spring seeps through the landslide deposits into QM5. SP-1 Spring is hydraulically connected to the landslide deposit. Anecdotal data also support the hydraulic connection between SP-1 Spring and the landslide deposits. The travel time to QM5 is 11 days. The estimated flow rate is approximately 70 feet/day based on the first arrival of the dye. However, because the travel time was calculated from the results of dye receptors, the detection time could be earlier. The flow rate based on the time to the peak concentration is approximately 40 feet/day. Because of the combined flow route, this value is not meaningful.

9.4.5.3 Connection from Sinking Stream SS-4 to SP-1 Spring

Sinking stream SS-4 is 50 feet away from the quarry wall, where the water sinks into the surface through a sinkhole. However, no leakage of water was visible on the quarry wall. Approximately 1 kg of Fluorescein was introduced into the creek. The dye was detected at SP-1 Spring in the dye receptors collected 66 days after the dye injection. Since then the dye was detected in most of the dye receptors at SP-1 Spring until the end of the second phase monitoring (Fig. 9.7). The detected dye concentration is over ten times the background. The peak concentration occurred in the dye receptor collected on May 28, 2004, approximately 87 days after the injection. No breakthrough curve was established for this dye at SP-1 Spring because the dye concentration is below the quantitation limit for all the water samples. The map distance between the sinking point of SS-4 and SP-1 Spring is approximately 2900 feet. The average flow rate from SS-4 to SP-1 Spring was estimated to be 40 feet/day based on the first arrival of the dye. Because the water from SS-4 has to travel over 400 feet vertically to reach the saturated zone and the detection time was calculated from a weekly sampling frequency, the flow rate is not accurate and may represent the lower limit. The flow rate was estimated to be 30 feet/day based on the peak concentration in the dye receptors.

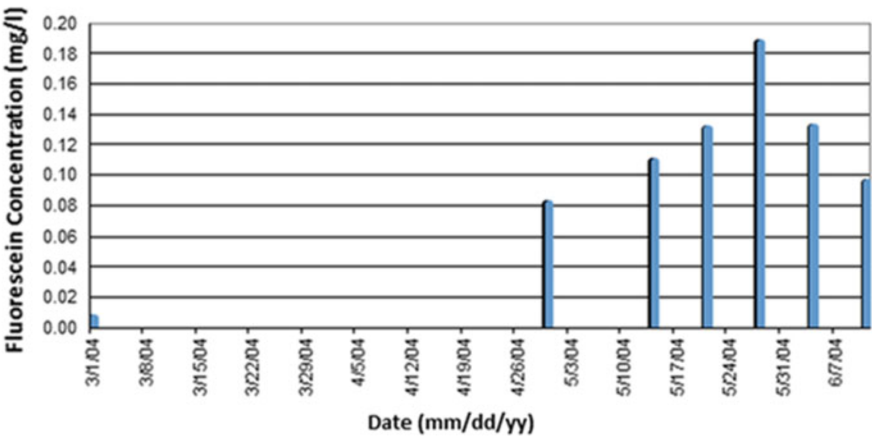

Fig. 9.7 Fluorescein dye laboratory results for dye receptors at monitoring well QM5

9.4.5.4 Connection from SS-4 to Monitoring Well NZA

Fluorescein was detected at NZA 45 days after the dye injection. The positive detection lasted three weeks. The peak concentration in the receptors occurred 52 days after the injection. Since the dye was detected at NZA before SP-1 Spring and the dye concentration at NZA appears to be higher than that at SP-1 Spring, it is possible that the water flows to NZA first and then moves to SP-1 Spring. However, it is also possible that the water takes a different route to NZA. The map distance between the sinking point of SS-4 and NZA is approximately 2,200 feet. The flow rate from SS-4 to NZA was approximately 50 feet/day based on the first arrival of the dye. Based on the peak concentration of the dye, the flow rate was estimated to be 40 feet/day.

9.4.5.5 Connection from Sinking Stream SS-2 to SP-3 Spring

A hydraulic connection was established between the sinking stream SS-2 and SP-3 Spring. Six days after Eosine dye was introduced into SS-2, it was detected at SP-3 Spring. As shown in the breakthrough curve (Fig. 9.8), the dye concentration increased very rapidly after its detection and reached its peak in 13 days after the dye injection. The presence of the dye is very persistent, and its concentration decreases gradually. The concentration in the dye receptors also indicates persistence of the dye at SP-3. The map distance between SS-2 and SP-3 Spring is approximately 4,200 feet. The flow rate was estimated to be 700 feet/day based on the first arrival of the dye. The flow rate was estimated to be 320 feet/day based on the time to reach the peak concentration.

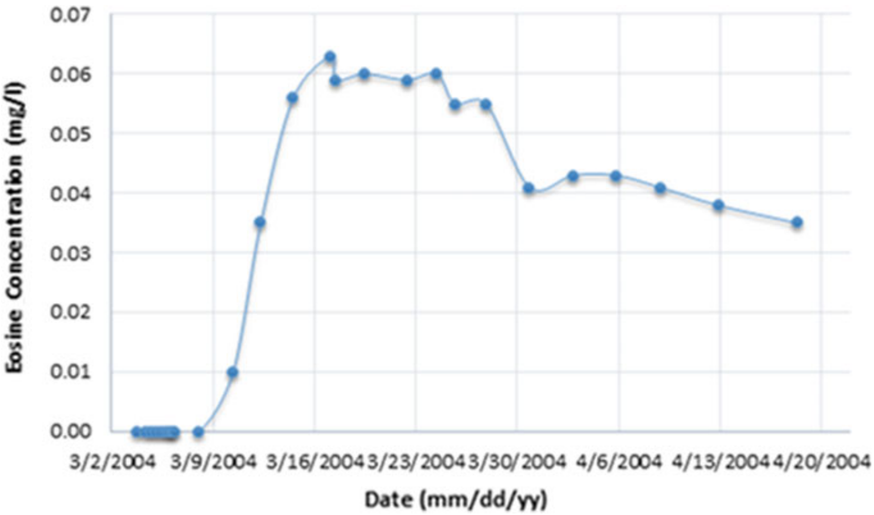

Fig. 9.8 Fluorescent dye eosine laboratory results for water samples at SP-3 spring

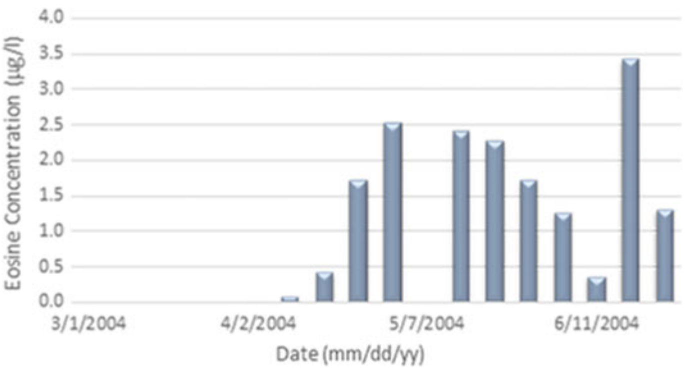

Fig. 9.9 Fluorescent dye eosine laboratory results for dye receptors at M1B

9.4.5.6 Connection from Sinking Stream SS-2 to Monitoring Well M1B

Eosine dye was detected 38 days after its injection at monitoring well M1B. The presence of the dye was persistent, and it was detected in most of the dye receptors that were collected after the first positive detection (Fig. 9.9). The peak concentration of the dye occurred on June 18, 2004, approximately 106 days after the dye injection. The map distance between the sinking point of SS-2 and M1B is approximately 3000 feet. Based on the first arrival of the dye, the flow rate was estimated to be 80 feet/day. Based on the time to reach peak concentration, however, the flow rate was estimated to be 30 feet/day.

9.4.5.7 Connection from Sinkhole SH-6 to SP-1 Spring

Rhodamine WT was injected into sinkhole SH-6. The dye was detected 3.3 days later in the water sample at SP-1 Spring. A dye breakthrough curve was established for the dye at SP-1 Spring (Fig. 9.10). The dye concentrations for all the samples were relatively low, but the curve is a typical breakthrough curve from a tracer test. The dye concentration increased relatively rapidly and reached its peak in approximately 10 days. The dye recession process was slow, and it lasted over a month before getting back to the non-detectable level. The dye was also detected in the dye receptors. The dye was not positively detected in the receptors until 16 days after the dye injection. The map distance between SH-6 and SP-1 Spring is 4100 feet. The flow rate from the Sinkhole Plain to SP-1 Spring could be 1240 feet/day based on the first arrival of the dye in the water samples. Based on the time to the peak concentration in the breakthrough curve, the flow rate was estimated to be 410 feet/day.

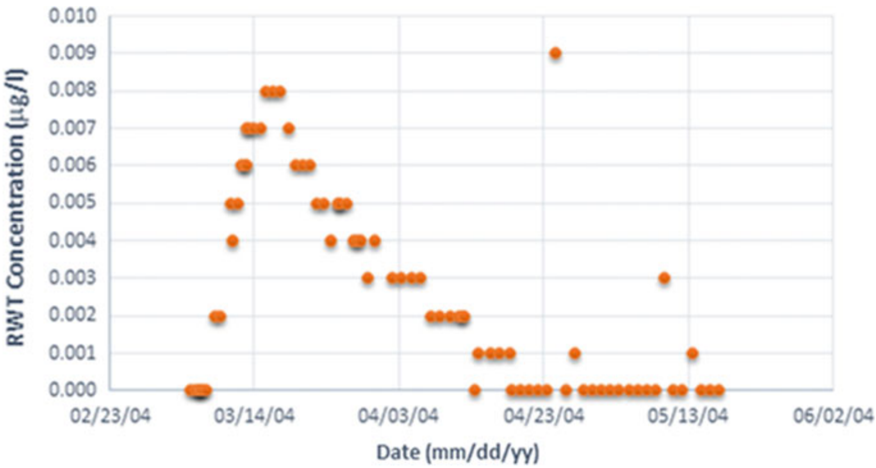

Fig. 9.10 Fluorescent dye Rhodamine WT laboratory results for water samples at SP-1 Spring

9.4.5.8 Connection from Sinkhole SH-6 to Monitoring Well NZA

Rhodamine WT was positively detected at NZA in the dye receptors 45 days after the dye injection. The peak concentration in the dye receptors also occurred 45 days after the dye injection. The dye concentrations were generally lower than those in SP-1 Spring. It seems that the water in the sinkhole area that flows to SP-1 Spring may not flow through the fracture system intercepted by NZA. It is possible that more than one fracture system is present in the saturated zone of the aquifer. The distance between SH-6 and NZA is approximately 3,250 feet. The estimated flow rate was 72 feet/day based on either the first arrival of the dye or the peak concentration of the dye.

9.4.5.9 Possible Connection from Sinkhole SH-6 to Monitoring Well M5A

The dye receptor collected at M5A on April 11, 2003, had a Rhodamine WT concentration of 0.3 µg/l, which is over 6 times the background value (0.047 µg/l). In most of the dye receptors collected in the following weeks, the dye concentration stayed at the same level. The hydraulic connection between M5A and SH-6 is probably valid. M5A is approximately 1300 feet west from SH-6. The flow rate based on the first arrival of the dye was estimated to be 30 feet/day. The flow rate based on the peak concentration of the dye was also approximately 30 feet/day.

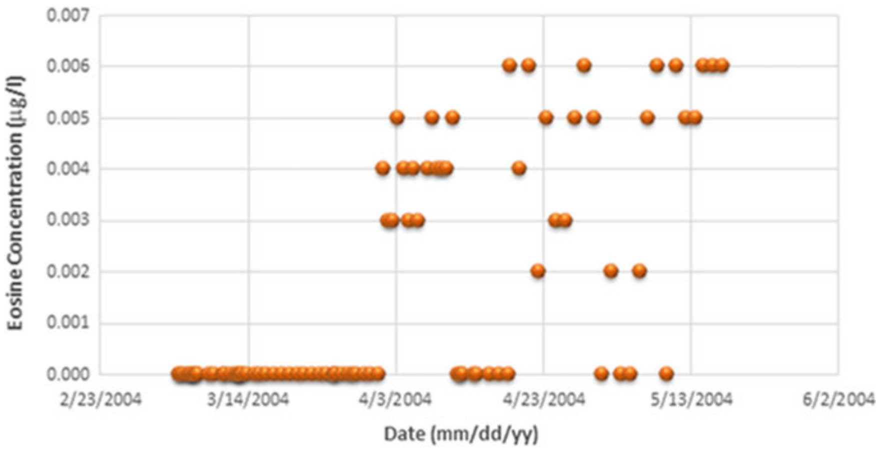

Fig. 9.11 Fluorescent dye eosine laboratory results for water samples at SP-1 spring

9.4.5.10 Possible Connection from Sinking Stream SS-2 to SP-1 Spring

Eosine was not positively detected in any of the dye receptors at SP-1 Spring. However, analysis from the water samples indicates an erratic dye breakthrough curve, as shown in Fig. 9.11. The Eosine dye had been below the detection limit until April 1, 2003 when its concentration increased to 0.004 μg/l. The concentration stayed at this level for approximately 9 days and then it dropped below the detection limit. A similar episode was repeated for subsequent water samples. The erratic nature of the curve is probably caused by the low concentration of the dye in the water samples. Although a definite hydraulic connection cannot be established between SS-2 and SP-1 Spring from the breakthrough curve, it is highly possible that water at SS-2 flows to SP-1 Spring. Well M1B in the saturated zone had already had a positive detection of the Eosine dye. The distance between SS-2 and SP-1 Spring is approximately 5400 feet. The estimated flow rate based on the first arrival of the dye from SS-2 to SP-1 Spring was 190 feet/day.

9.4.5.11 Connection from Sinking Stream SS-1 to SP-1 Spring

This connection between sinking steam SS-1 and SP-1 Spring was confirmed by injecting Fluorescein dye at SS-1 in the third phase of the dye tracing. Fluorescein was positively detected in the receptors 13 days after the dye injection. The maximum concentration of fluorescein in the dye receptors occurred three weeks after the dye injection. A small amount of Fluorescein was still detectable until January 7, 2005. The Fluorescein was also detected in the water samples. The breakthrough curve is shown in Fig. 9.12. The first water sample in which the Fluorescein dye was detected was collected at 11:00 p.m., August 24, 2004, 6.5 days after the dye injection. The

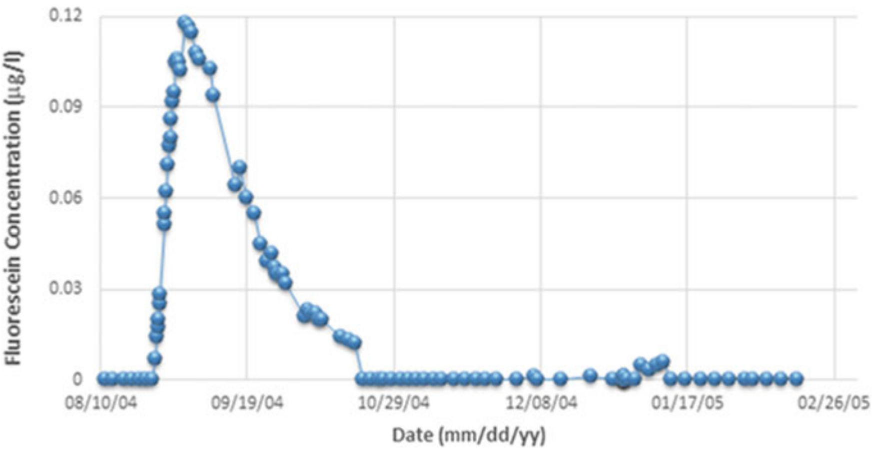

Fig. 9.12 Fluorescent dye Fluorescein laboratory results for water samples at SP-1 Spring

peak concentration occurred on September 3, 2004, i.e. 16 days after the dye injection. After the peak concentration, the Fluorescein concentration dropped gradually to the background level. The breakthrough curve is typical of karst aquifers in which conduit/fracture flow dominates.

The map distance between where the dye was injected at SS-1 and SP-1 Spring is approximately 4900 feet. The breakthrough curve established from the water samples was used to estimate the approximate flow rate for the connection. The flow rate based on the first arrival of the dye was estimated to be 754 feet/day. The flow rate based on the time to reach peak concentration in the water samples was estimated to be 310 feet/day.

9.4.5.12 Connection from Sinking Stream SS-1 to SP-3 Spring

The connection between sinking stream SS-1 and SP-3 Spring was also confirmed by the injection of Fluorescein dye at SS-1 in the third phase of the dye tracing. Figure 9.13 shows the laboratory results for water samples. The first water sample in which the Fluorescein dye was detected was collected on August 22, 2004, 4.125 days after the dye injection. The peak concentration occurred on August 26, 2004, 7.83 days after the dye injection. After the peak concentration, the Fluorescein concentration dropped gradually to the background level. The breakthrough curve is typical of karst aquifers in which conduit/fracture flow dominates. The Fluorescein was detected in the dye receptors also.

The map distance between where the dye was injected at SS-1 and SP-3 Spring is approximately 3,700 feet. The breakthrough curve established from the water samples was used to estimate the approximate flow rate for the connection. The flow rate of the groundwater based on the first arrival of the dye was estimated to be

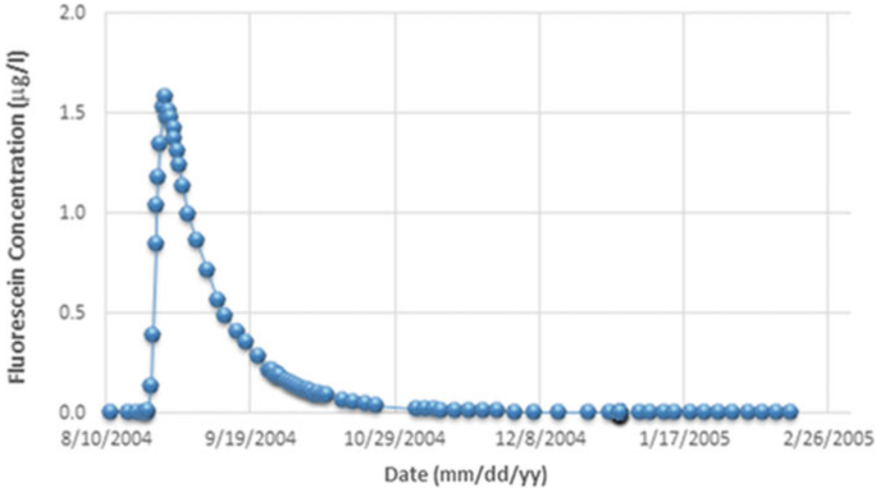

Fig. 9.13 Fluorescent dye fluorescein laboratory results for water samples at SP-3 spring

900 feet/day. The flow rate based on the time to reach the peak concentration was estimated to be 470 feet/day.

9.4.5.13 Connection from Sinking Stream SS-1 to Monitoring Well M1B

The connection between sinking stream SS-1 and monitoring well M1B was also detected from the injection of Fluorescein dye at SS-1 in the third phase of the dye tracing. Figure 9.14 shows the breakthrough curve for the dye receptors. The

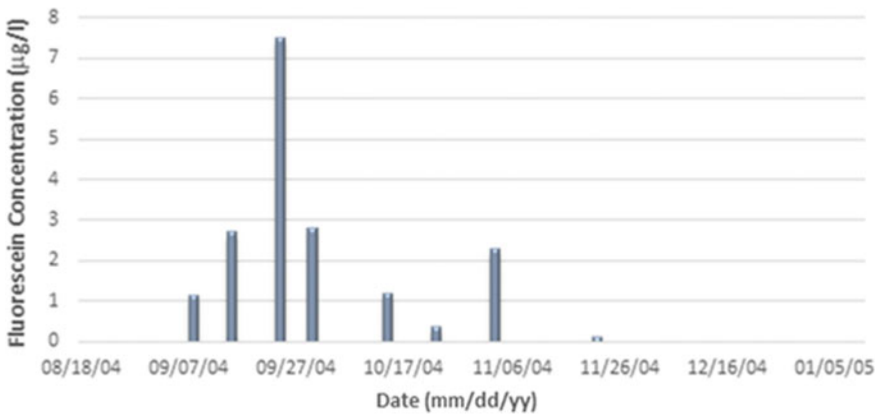

Fig. 9.14 Fluorescent dye Fluorescein laboratory results for dye receptors at M1B

Fluorescein dye began to show up in the dye receptors collected 21 days after the injection. The maximum concentration occurred 37 days after the dye injection. The dye was detectable in the dye receptors until November 3, 2004. The map distance between SS-1 to M1B is approximately 2,500 feet. Based on the first arrival of the dye, the flow rate for this connection was estimated to be 120 feet/day. Based on the time to reach the peak concentration in the dye receptors, the flow rate was estimated to be 70 feet/day.

9.4.5.14 Connection from Sinking Stream SS-1 to M5A

The connection between SS-1 and monitoring well M5A was also proven by the injection of Fluorescein dye at SS-1 in the third phase of the dye trace. Figure 9.15 shows the breakthrough curve for the dye receptors. The Fluorescein dye began to show up in the dye receptors collected 18 weeks, 126 days after the injection. The dye concentration was relatively small but more than 10 times the quantitation limit of 0.005 μg/l. The maximum concentration occurred in the dye receptor collected on January 8, 2005. The map distance from SS-1 to M5A is approximately 3,400 feet. The flow rate for this connection was estimated to be 30 feet/day if the time was based on the first arrival of the dye. If the time to reach the peak concentration of the dye was used in the calculation, the flow rate was estimated to be 20 feet/day. Because Fluorescein dye was also used at sinking stream SS-4 on March 3, there is a slight possibility that the Fluorescein detected at M5A came from SS-4. If this is the case, the travel time from SS-4 to M5A was approximately 293 days, indicative of a very slow rate of the groundwater flow. Based on all the other data, the former interpretation is much more probable.

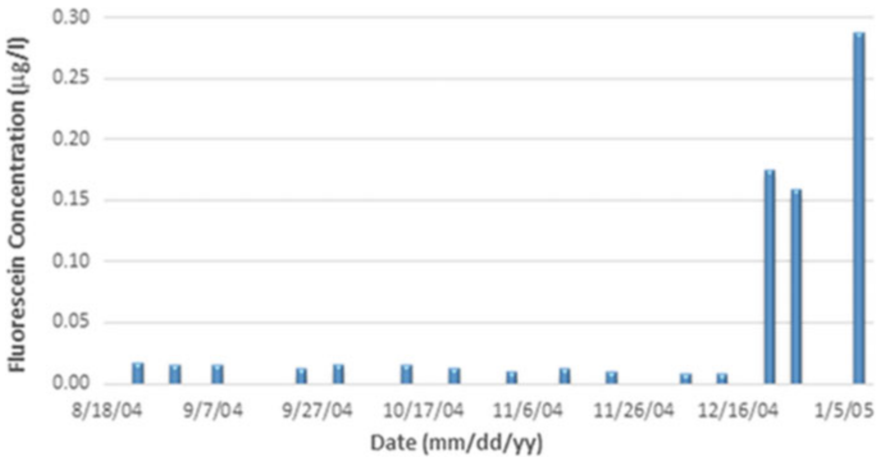

Fig. 9.15 Fluorescent dye fluorescein laboratory results for dye receptors at M5A

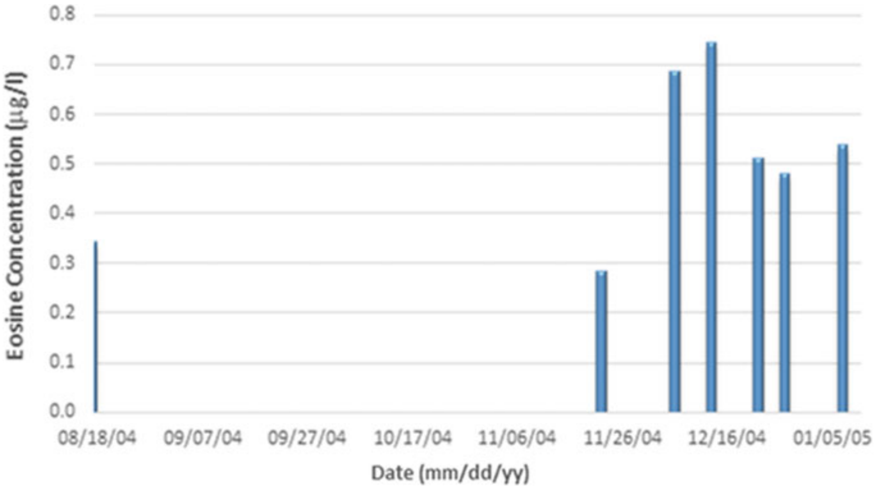

Fig. 9.16 Fluorescent dye eosine laboratory results for dye receptors at SP-1 spring

9.4.5.15 Connection from Sinking Stream SS-8 to SP-1 Spring

The connection between sinking stream SS-8 and SP-1 Spring was detected by the injection of Eosine dye at SS-8 in the fourth phase of the dye tracing. Figure 9.16 shows the laboratory results for the dye receptors. The Eosine dye began to show up in the dye receptors collected on November 22, 2004, 67 days after the injection. The dye concentration is relatively small but more than 10 times the quantitation limit of 0.005 µg/l. The Eosine dye has been detectable in all the dye receptors collected after November 22, 2004. The maximum concentration occurred in the dye receptor collected on December 13, 2004. The map distance between SS-8 to SP-1 Spring is approximately 2.75 miles, or 14,520 feet. The flow rate for this connection was estimated to be 220 feet/day if the time was based on the first arrival of the dye. If the time to reach the peak concentration of the dye was used in the calculation, the flow rate was estimated to be 160 feet/day. A breakthrough curve was not established at SP-1 Spring because the concentrations of the Eosine dye in all the water samples were below the quantitation limit of 0.01µγ/l.

9.4.5.16 Connection from Sinking Stream SS-8 to SP-3 Spring

The connection between sinking stream SS-8 and SP-3 Spring was also detected by the injection of Eosine dye at SS-8 in the fourth phase of the dye tracing. Figure 9.17 shows the laboratory results for the dye receptors. The Eosine dye began to show up in the dye receptors collected on November 22, 2004, i.e. 67 days after the injection. The dye concentration in the dye receptor at SP-3 Spring is generally one magnitude larger than the concentration of the receptor collected at the same time as SP-1 Spring.

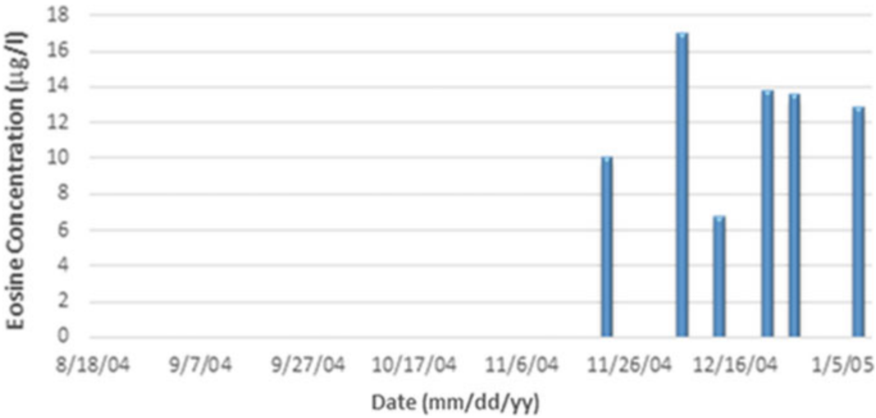

Fig. 9.17 Fluorescent dye eosine laboratory results for dye receptors at SP-3 spring

The Eosine dye has been detectable in all the dye receptors collected after November 22, 2004. The maximum concentration occurred in the dye receptor collected on December 6, 2004. The map distance from SS-8 to SP-3 Spring is approximately 2.63 miles, or 13,860 feet. The flow rate for this connection was estimated to be 210 feet/day if the time was based on the first arrival of the dye. If the time to reach the peak concentration of the dye was used in the calculation, the flow rate was estimated to be 170 feet/day. A breakthrough curve was not established at SP-3 Spring because the concentrations of the Eosine dye in all the water samples were below the quantitation limit of 0.01μγ/l.

9.4.5.17 Connection from Sinking Stream SS-8 to Spring SP-21

The connection between sinking stream SS-8 and spring SP-21 was also established by the injection of Eosine dye at SS-8 in the fourth phase of the dye tracing. Figure 9.18 shows the laboratory results for the dye receptors. The Eosine dye began to show up in the dye receptors collected on October 15, 2004, approximately one month after the injection (29 days). The Eosine dye has been detectable in all the dye receptors collected since then, with concentrations often being over 100 μg/l. The maximum concentration of 443 μg/l occurred in the dye receptor collected on November 13, 2004. The map distance from SS-8 to SP-21 is approximately 1.13 miles, or 6,000 feet. If the time was based on the first arrival of the dye, the flow rate for this connection was estimated to be 210 feet/day, which is the same as the flow rate calculated for the flow from SS-8 to SP-3 Spring. If the time to reach the peak concentration of the dye was used in the calculation, the flow rate was estimated to be 100 feet/day.

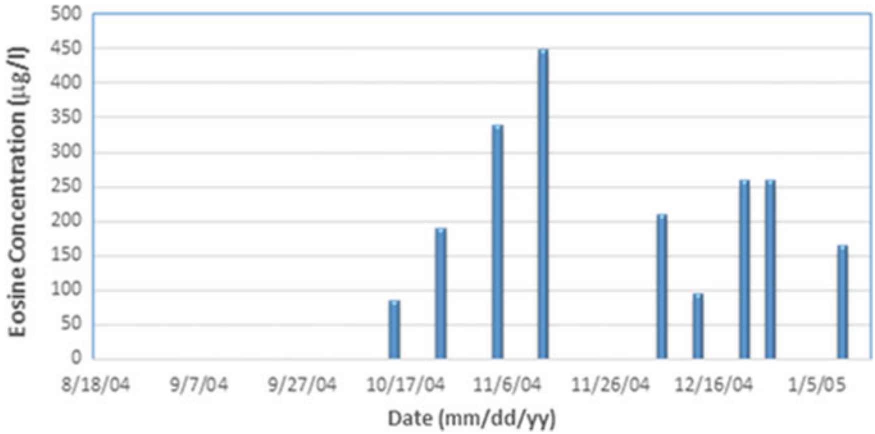

Fig. 9.18 Fluorescent dye Eosine laboratory results for dye receptors at spring SP-21

9.4.5.18 Connection from Sinking Stream SS-8 to Monitoring Well M1B

The connection between sinking stream SS-8 and M1B was also established by the injection of Eosine dye at SS-8 in the fourth phase of the dye tracing. Figure 9.19 shows the laboratory results for the dye receptors. The Eosine dye began to show up in the dye receptors collected on October 23, 2004, approximately 37 days after the injection. The Eosine concentrations in the receptors are less than 1 µg/l and the dye has been consistently detectable in the dye receptors collected since then. The maximum concentration occurred in the dye receptor collected on November 3, 2004. The map distance between SS-8 to M1B is approximately 2.3 miles, or 12,100 feet.

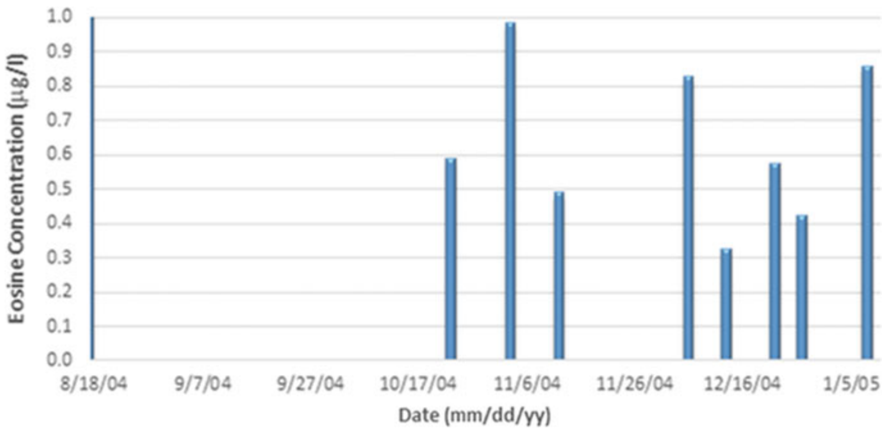

Fig. 9.19 Fluorescent dye eosine laboratory results for dye receptors at monitoring well M1B

If the time was based on the first arrival of the dye, the flow rate for this connection was estimated to be 330 feet/day. If the time to reach the peak concentration of the dye was used in the calculation, the flow rate was estimated to be 250 feet/day.

9.4.6 Summary of Dye Tracing

Table 9.5 summarizes the hydraulic connections established by the dye tracing and the estimated flow rates from the dye injection point to the monitoring point. The estimated flow rates were calculated from the tracer travel times (first dye detection and peak concentration) and the map distance between the two points. The flow rates can only be considered as an approximation. In addition, the flow rates vary with time. They can significantly increase in response to rain events. Nevertheless, these traces provide the essential information on the extent to which the various sinkholes, sinking points, or injection points are connected to SP-1 Spring or SP-3 Spring.

- Based on the tracing tests conducted in this study, SP-1 Spring is hydraulically connected to sinking streams SS-8, SS-1, SS-2, and SS-4, sinkhole SH-6, and monitoring well NZA.
- SP-3 Spring is hydraulically connected to sinking streams SS-8, SS-1, and SS-2.
- Monitoring well M1B is hydraulically connected to sinking streams SS-8, SS-1, and SS-2,
- Monitoring well NZA is hydraulically connected to sinkhole SH-6 and sinking stream SS-4.
- Monitoring well M5A is hydraulically connected to sinkhole SH-6 and sinking streams SS-1 and SS-4.

9.5 Conceptual Site Model for SP-1 Spring

In non-karst terranes there is a clean distinction between surface water and groundwater, and between surface drainage basins and groundwater aquifers. Drainage basins, which determine the catchment and runoff characteristics of surface water are defined by drainage divides set by local topography. Surface water is often only loosely coupled to groundwater system because of the slow rate of infiltration. These conceptual distinctions between basins and aquifers are blurred in karst areas like the one under study because of the integrated system of solution-enlarged fractures or conduits that carry water through the subsurface. Localized recharge to the conduit system occurs where surface streams sink underground and where sinkholes collect overland flow and direct it to the subsurface. The discharge of water from the conduit system often takes place at one or several large springs that often form the headwaters of a perennial surface stream. In karst there is a much more intimate relationship between groundwater and local surface water than in other types of aquifers.

9.5.1 Recharge Sources for SP-1 Spring

The boundaries of the delineated catchment basin for SP-1 Spring are determined from the data collected during this tracer study, the understanding of the local geology, and surface drainage patterns. The boundaries in the non-karst areas are based on the topographic divides. The SP-1 Spring catchment basin cannot be absolutely separated from the SP-3 Spring catchment basin because they share the water from SS-1, SS-2, and SS-8. These two catchment basins are hydraulically connected.

The data collected in this tracer study clearly indicate that SP-1 Spring receives recharges from sinking streams SS-8, SS-1, SS-2, and SS-4. Part of the water that sinks at SS-8 recharges SP-1 Spring, and part of the water re-emerges downstream at SP-21. During high-flow seasons, the surface waters flow past the sinking points, and only a percentage of the flow in each creek recharges the groundwater. During low-flow conditions, most of the water that sinks at SS-1 and SS-2 recharges SP-1 Spring. SP-1 Spring also receives water from SS-4, where most of the water sinks underground through a sinkhole.

Because of the uncertainties in the headwaters for the sinking streams, the total recharge area for SP-1 Spring and SP-3 Spring cannot be precisely computed. If the surface drainage areas of these sinking creeks are included in the catchment basin of SP-1 Spring, the total catchment area is approximately 3 mile^2, or 2,000 acres. This is not the catchment area solely for SP-1 Spring. A portion of the water in the catchment basin flows to SP-3 Spring and Springs SP-21. In addition, during high-flow seasons, a portion of the water in the surface creeks flows through the catchment basin and continues downstream. Therefore, SP-1 Spring gets its recharge from the delineated catchment area; however, not all the water in the basin flows to SP-1 Spring. The delineated catchment basin is an “open” basin, rather than a “closed” one.

Like any other karst aquifer, the marble aquifer includes input from surface catchments on non-karstic rocks such as the Santa Margarita Sandstone, granitic rocks, and schist. These non-karstic, but hydrologically connected rocks are referred to as “borderland.” Surface runoff from the borderlands drains through surface streams that flow onto the karst area, where some sink underground at the margin of the marble or as they flow over the marble outcrop. These are the sinking stream inputs to the karst groundwater system. Little runoff is present on the karst land, which is typical in well-developed karst terranes. Overland flow during storms disappears into sinkholes to enter the groundwater system as internal runoff.

Depending on where the water comes from, the recharge sources to SP-1 Spring can be divided into two categories—allogenic recharge and autogenic recharge. Allogenic recharge derives its water from a neighboring non-karst borderland, whereas auotogenic recharge derives its water from precipitation falling on the karst land. Table 9.6 lists the various recharge sources to SP-1 Spring.

Based on the geologic map by Brabb (1989), the autogenic recharge area is approximately 200 acres and the allogenic recharge area is approximately 1800 acres. Thus, the recharge area for SP-1 Spring consists of approximately 10% karst land and 90% borderland. The existing quarry and the amendment area cover approximately 106

Table 9.6 Recharge sources for SP-1 Spring

Recharge sources		Descriptions
Allogenic recharge	Sinking streams	The groundwater tracing investigation has identified four such sinking streams that are hydraulically connected to SP-1Spring and/or SP-3 Spring. These four sinking streams are SS-8, SS-1, SS-2, and SS-4. The headwaters of these sinking streams have not been determined but likely from granitic rocks and/or on the Santa Margarita Sandstone southwestern side of Ben Lomond Mountain
	Sinkhole	Many sinkholes have been reported in the study area. The most significant sinkholes are on a sinkhole plain where dye tracing in one of the sinkholes (SH-6) indicates that this area is hydraulically connected to SP-1 Spring. The estimated flow rate is over 1,000 feet/day based on the first arrival of the injected dye at SP-1 Spring, whereas the estimated flow rate is approximately 410 feet/day based on the time at the peak concentration of the dye at SP-1 Spring. The sinkhole plain is developed over the marble but at the contact with Santa Margarita Sandstone. It collects water from the local surface areas and the discharges from springs. Because the main water sources are from the non-karstic borderland, the recharge at the sinkhole plain is considered to be allogenic
	Inter-aquifer transfer	Infiltration in the borderlands can produce aquifers in the non-karstic rocks. The water from these aquifers can move into the marble in the subsurface. No evidence is available for this inter-aquifer transfer; however, the marble is embedded in the granitic rock and is in contact with Santa Margarita Sandstone. The non-karstic aquifers located north and northeast have the potential to recharge the marble
	Landslide deposits	The tracer test at NZA and previous observations indicate that the landslide deposits and SP-1 Spring are hydraulically connected. When the water level in the landslide deposits is higher than that at SP-1 Spring, it is conceivable that SP-1 Spring gets recharge from the landslide

(continued)

Table 9.6 (continued)

Recharge sources		Descriptions
Autogenic recharge	Internal drainage through sinkholes	The dye tracing at sinkhole SH-11 does not indicate that this area is actively connected to SP-1 Spring. It is likely that the injected and the associated water are temporarily ponded in the unsaturated zone. Although the sinkhole has been reported to carry the overland runoff into the subsurface, it does not seem to have a drain that can efficiently carry the water to the saturated zone and then to SP-1 Spring. Water ponding at the bottom of a sinkhole is not uncommon (White 1988), especially in the study area where the saturated zone is underlain by over 300 feet of rocks that have fractures and voids
	Diffuse infiltration through soils and Santa Margarita sandstone	Rainwater may penetrate the soil on the karst surface as a diffuse infiltration. Observations on the quarry walls indicate that the soil–bedrock contact is irregular, and the marble consists of fractures that are filled with soil. Some soil-filled fractures have stains of water flow. The bedrock itself is relatively impermeable, and the open pathways available to carry water to the groundwater are limited to fractures. As a result, there is developed a temporary perched water body in what is called epikarst zone. The residence time in epikarst storage is typically weeks (Gunn, 1986; Williams, 1985), sometimes decades (Even et al. 1986) The epikarst zone, sometimes called the subcutaneous layer, is the dissolutionally weathered upper portion of the bedrock in carbonate landscapes. Epikarst zones store water seasonally or after major precipitation periods. Some sinkholes are discrete water input points into the epikarstic zone On the karst land, Santa Margarita Sandstone caps a small area. Exploratory boreholes indicate the presence of isolated water in the sandstone. Significant recharge to the marble from the caprocks does not seem to occur on an annual basis
	Quarry	The dye tracing at monitoring well NZA indicates that the water below the quarry floor is hydraulically connected to SP-1 Spring. Marble is exposed at the bottom of the quarry and the quarry floor collects rainwater. Standing water was observed on the quarry floor after rains. The marble itself has very low permeability, as indicated by the rudimentary aquifer tests in monitoring wells. If there is any water flowing into the saturated zone, the recharge is through fractures. Fine-grained "filtering" materials were placed on the quarry floor in 1998 to reduce the infiltration rate

acres in the karst land, which is approximately 5% of the total catchment area. The vast majority of the recharge for SP-1 Spring is allogenic.

The flow of SP-1 Spring has been measured intermittently since 1921. The annual average discharges for 1921, 1922, and 1931 ranged from 0.8 million gallons per day (mgd) to 1.2 mgd. The flow at SP-1 Spring for the period between 1961 and 1965 varied from 1 mgd to 1.34 mgd. These measurements were taken prior to 1968 when the quarry was opened. From 1988 to 1997, the discharge data are based on the production volumes at SP-1 Spring and the annual average flow varied from 0.76 mgd to 1.31 mgd, although not all the flow was measured. The time frames in which valid discharge data are available for 1999, 2000, 2002, 2003, and 2004, and their annual average flows were estimated to be 2.01 mgd, 1.07 mgd, 1.13 mgd, 1.41 mgd, and 1.53 mgd, respectively. Based on the aforementioned data, the annual average flow ranges at SP-1 Spring have been comparable before and after the quarry was in operation.

9.5.2 Groundwater Pathways to SP-1 Spring

In the marble, water is present in both an unsaturated zone and a saturated zone, as indicated by the groundwater monitoring data and isotope data and as supported by the groundwater tracing investigation. SP-1 Spring drains the water from the saturated zone that is characterized by fracture/conduit flow. The unsaturated zone is highly fractured and well developed. Many voids (including caves) are present. Isolated water levels exist, as measured in the monitoring wells that are screened in the unsaturated zone. Because of the great thickness of the unsaturated zone and the high porosity value, it has a great capacity for storing water. Following infiltration through topsoil and internal runoff through sinkholes on the karst land, water can be collected and temporarily stored in the unsaturated zone, until it subsequently recharges the saturated zone. A small proportion of water recharged at sinking stream SS-1 and the sinkhole plain may flow into the unsaturated zone, as indicated by the possible hydraulic connections between SS-1 and M5A and SH-6 and M5A. However, these connections are relatively poor, with the flow velocities ranging from 20 to 30 feet/day.

The data collected during this tracer study do not indicate a strong hydraulic connection between the unsaturated zone and the saturated zone. Two tracing tests through sinkhole SH-11 did not yield any positive detection of the dyes at SP-1 Spring and SP-3 Spring. Table 9.7 lists the main characteristics of the karst water system and their supporting evidence.

Like any other karst aquifer, the groundwater flow in the saturated zone of the marble ranges from conduit flow to diffuse flow. The flow is convergent to SP-1 Spring. The flow is concentrated into larger conduits closer to the spring. Although it is impossible to pinpoint the exact locations of the active conduits, the dye tracing data indicate that they may be located at, or near, NZA and M1B. The active conduits often lie very close to the local drainage level as observed in many active karst systems

Table 9.7 Main characteristics of the karst water system

Karst water system	Main characteristics	Supporting data
Saturated zone	Conduit/fracture flow. The saturated zone is heterogeneous and consists of multiple flow paths with different flow velocities. The groundwater flow is convergent toward SP-1 Spring through major conduits that are fed by water from small fractures	• A fracture zone was observed in monitoring well NZA • The tracer test at Monitoring Well NZA clearly demonstrated the karst feature of the saturated zone • The dye tracing at SH-6, SS-1, and SS-8 indicated a quick flow to SP-1 Spring • Relatively slow flow was observed from the tracing test at sinking stream SS-4 • Two monitoring wells in the saturated zone of the marble in the existing quarry and amendment area showed positive dye detection • The estimated flow rates range from 30 feet/day to 2,760 feet/day
	Strong hydraulic connection to allogenic recharge	• The water from SS-4 sinks vertically to the saturated zone • The tracing test at SS-4 is hydraulically connected to NZA and SP-1 Spring • The dye tracing at SS-2 is hydraulically connected to M1B (well in saturated zone) • The dye tracing at SH-6 is hydraulically connected to NZA • The dye tracing at SS-1 is hydraulically connected to M1B • The dye tracing at SS-8 is hydraulically connected to M1B
Unsaturated zone	High storage capacity	• Frequently encountered voids in boreholes • Presence of shallow caves • Thick unsaturated zone • Consistent presence of water over years in several monitoring wells such as BD40, BD41, BD44, M3A, and M6B
	Weak hydraulic connection to saturated zone	• Different water levels between wells in saturated zone and those in unsaturated zone. Water level in unsaturated zone is consistently higher than that in saturated zone • Different isotope signatures between the water samples in saturated zone and those in unsaturated zone. The water samples in unsaturated zone appear to be impacted by evaporation • Different conductivity values between the water samples in saturated zone and unsaturated zone. The water in unsaturated zone tends to have longer residence time • The tracing tests at SH-11 had a negative detection of the dye at SP-1 Spring and the monitoring locations. M1A and M1B are only a few tens of feet away from SH-11, no dye was detected in either of them

(White 1993). Vertical shafts or solution-widened fractures often develop along the borders between karst land and the borderland. The majority of the water draining from surface catchments, such as the karst of the Mammoth Cave area of Kentucky or of the Cumberland Mountains of Tennessee and northern Alabama often takes a direct route through the unsaturated zone to the underlying conduit system (White, 1988; Smart and Campbell 2003). The continuous uplift of the coastal areas may further enhance the development of the vertical shafts in the study area. At sinking stream SS-4, for example, the surface water sinks into the ground, and no water is visible on the adjacent quarry wall that is over 300 feet tall and only 50 feet away from the sinking point. At sinking stream SS-1, preliminary exploration of a cave indicated the possibility of a deeper passageway.

The geologic structure and the tracing tests suggest quick flow from SS-8, SS-1, and sinkhole SH-6 to SP-1 Spring. During recharge events, water can flow into the conduit system and quickly move to SP-1 Spring. During the tracing tests, the majority of the water in SS_8 arrived at SP-1 Spring in approximately 88 days; the majority of the water in SS-1 arrived at SP-1 in approximately 20 days, while the majority of the water in the SH-6 area arrived at SP-1 Spring in approximately 10 days. The quickest water flow was detected between monitoring well NZA and SP-1 Spring, where most of the water arrived at SP-1 Spring in approximately 7.5 h. Unlike the sinking creeks, NZA is only a monitoring well in the groundwater flow paths, and it is not a source of water for SP-1 Spring.

The approximately 3-month travel time from sinking stream SS-8 to SP-1 Spring may correspond with the observed lags in the seasonal fluctuations of SP-1 Spring, as noted by Todd (1963). In his report, Todd has the following description of the lag: “December is the maximum rainfall month in the area, but the peak spring flow is in March. Similarly, August is the minimum rainfall month before the increase in the fall months, yet November is the month for minimum discharge.”

However, SS-8 is only one of the recharge sources for SP-1 Spring. While the recharge from SS-8 explains the seasonal fluctuation of water flow, other sources such as sinking stream SS-1 and the sinkhole SH-6 area, may explain the daily fluctuation of the water flow.

The karst aquifer also includes input from SS-4, SS-2, non-karstic aquifers in the borderland, small fractures around the conduits, and the unsaturated zone. These inputs occur through tight fractures in the low permeability rock in which the conduits are dissolved. They get recharged during the wet season. During dry periods, the water in these fractures gradually flows toward the conduits because the conduits provide pathways of the least resistance. This often forms a groundwater trough over the conduits. The recharge from the diffuse inputs helps sustain the flow at SP-1 Spring during dry seasons.

A conceptual diagram is presented in Fig. 9.20 to schematically illustrate the groundwater flow components and the complicated arrangement of flow paths brought on by the interplay between surface water and groundwater. This schematic diagram is not drawn to a specific scale, and the vertical profile is exaggerated. The lateral extent could range from several hundred feet to several miles. Because of the lack of information in the area between SS-8 and SP-1 Spring, this diagram is likely

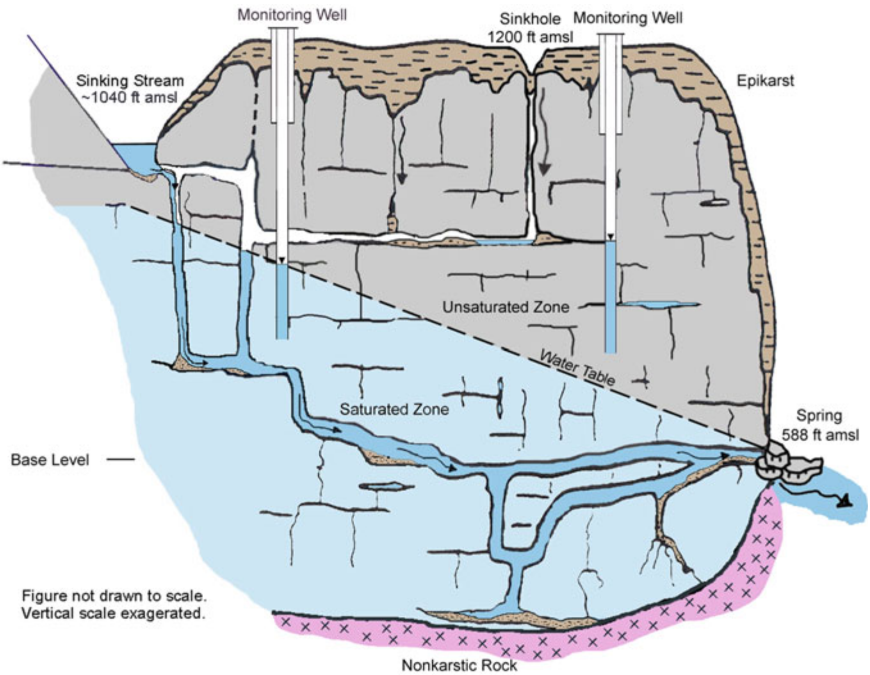

Fig. 9.20 Schematic conceptual site model for recharge source and flow paths to SP-1 spring

more representative of the flow conditions from SS-1 and SS-2 to SP-1 Spring. The water table fluctuates with the seasons.

9.6 Geochemical Characteristics at SP-1 Spring

9.6.1 Ionic Water Types

Figure 9.21 are trilinear plot of mineral analyses for approximately 20 different sources of water in the study area. The figure highlights two groups of samples that are representative of the marble and sandstone aquifers. Most area waters are of a calcium-bicarbonate type, including most streamflow. However, water associated with the marble aquifer is of a strongly calcium-bicarbonate type, with calcium comprising typically 75 percent or more of the major cations and sulfate comprising < 15 percent of the major anions (as milliequivalents per liter [meq/L]). The concentration of calcium in marble-aquifer groundwater is typically 6 to 13 times greater than the concentration of magnesium (as mg/L).

Water associated with the Santa Margarita Sandstone tends to be of a sodium-chloride or mixed type (e.g. springs along sinking streams SS-1 and SS-4). Water

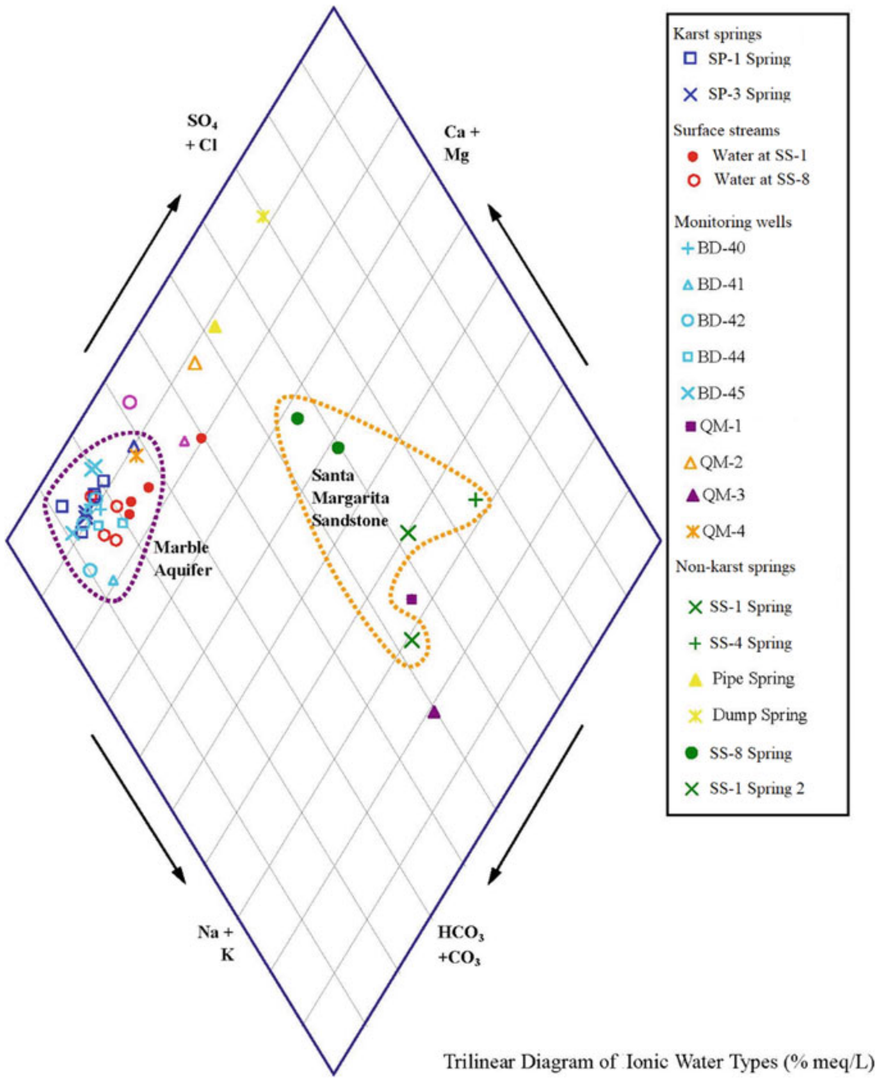

Fig. 9.21 Trilinear diagram of ionic water types

that has been in contact with stockpiled quarry waste tends to be of a calcium-sulfate type (Pipe and Dump springs, possibly QM-2,). Wells completed in granitic rocks near the downgradient boundary of the marble aquifer have a mixed-sodium water quality (QM-1 & -3).

9.6.2 Relationship Between Spring Discharge, Turbidity, Specific Conductance, and Temperature

9.6.2.1 Relationship Between Spring Discharge, Specific Conductance, and Temperature

The discharge, turbidity, specific conductance, and temperature have been monitored for many years at SP-1 Spring. Figure 9.22 shows their correlations for the data collected from 1998 to 2005. SP-1 Spring discharge ranged between 850 and 1100 gpm about 75 percent of the time. Water temperature provides a useful indicator of groundwater movement. The temperature of groundwater residing long-term within the aquifer typically approaches that of the mean annual air temperature (i.e. about 17.6 °C for the study area). Groundwater recharged by winter rainfall and runoff will reflect relatively cool temperatures for some period. Conversely, slow migrating groundwater will mimic seasonal air temperatures when approaching the ground surface, such as groundwater emerging from a seep. Figure 9.22d shows the correlation between SP-1 Spring discharge and water temperature during 2004–05. Spring flows below about 1100 gpm had little correlation with temperature whereas higher flows were generally greater than 16 °C, indicating that long-term groundwater storage contributes substantially to these flows.

Figure 9.22e shows the correlation between SP-1 Spring temperature and specific conductance. Flows with the lowest specific conductance (<400 microsiemens/centimeter [μS/cm]) are coldest (<15 °C) whereas flows with the highest specific conductance (>450 μS/cm) are warmest (>16 °C). Cold temperatures and relatively low mineral content reflect captured winter streamflow, whereas relatively warm water (approaching mean-annual air temperature) and higher mineral content reflect long-term groundwater storage. SP-1 Spring's discharge of relatively warm, mineralized water during peak flow conditions indicates a direct and substantial contribution from groundwater storage.

The water's specific conductance (i.e., electrical conductivity at 25 °C, expressed in μS/cm) is proportional to its concentration of total dissolved minerals. The recommended drinking water standard for specific conductance is 900 μS/cm, with enforceable limits set at 1,600 and 2,200 μS/cm.

Groundwater and surface water upgradient and cross gradient from the quarry marble aquifer tend to be low in dissolved minerals (<200 μS/cm). Water in contact with the marble becomes more mineralized and generally ranges between 300 and 1,000 μS/cm. Along major fracture zones east of the quarry, the dissolved mineral content tends to be relatively low in deep wells compared to nearby shallower wells (e.g., M6A vs. M6B, M1B vs. BD-44, M2A vs. M3B). Because dissolved mineral content usually increases with depth, this observation indicates that these deep wells encounter zones influenced by relatively rapid groundwater flow through deep karst conduits that drain stream swallow holes.

The average specific conductance of SP-1 Spring is approximately 480 μS/cm, which is intermediate between groundwater derived from captured streamflow

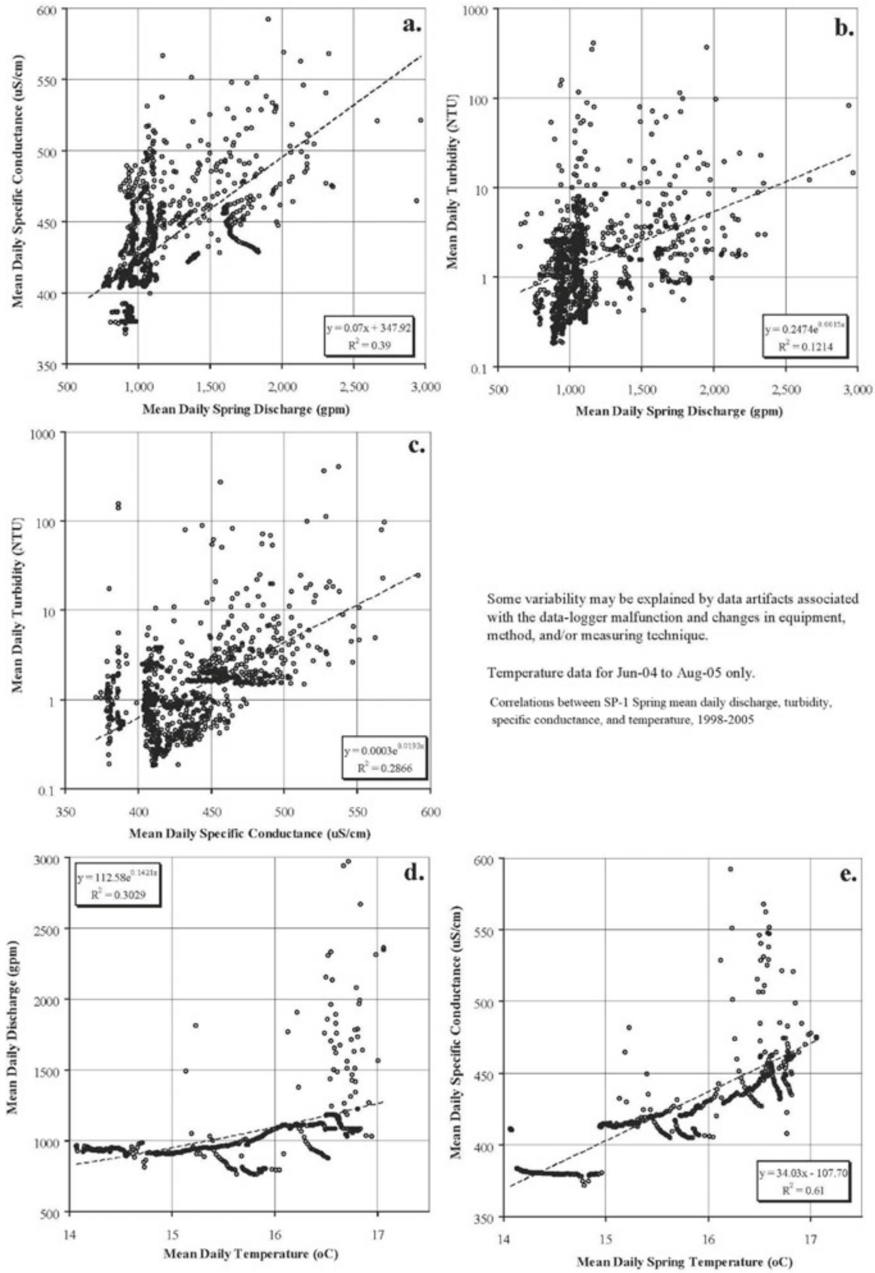

Fig. 9.22 Scattered plots between discharge, turbidity, specific conductance, and temperature at SP-1 spring **a** Relationship between specific conductance and spring discharge; **b** Relationship between turbidity and spring discharge; **c** Relationship between specific conductance and turbidity; **d** Relationship between temperature and spring discharge; Relationship between specific conductance and spring temperature

(generally 300–400 μS/cm) and more mineralized groundwater migrating relatively slowly from other sources of recharge. If it is assumed that upgradient groundwater has an average specific conductance of 600 μS/cm, then a roughly 50:50 mix of captured streamflow and upgradient groundwater is needed to produce the average specific conductance of SP-1 Spring.

The specific conductance of SP-1 Spring and discharge quickly rise to greater than 600 μS/cm during storm periods and gradually decline after each storm and throughout the dry season. This gradual recession is also apparent in the mean daily specific conductance duration curve. The scatter plot in Fig. 9.22a illustrates the direct, albeit rough, correlation between the spring's specific conductance and discharge. This trend is the opposite of that typically exhibited by streamflow, in which specific conductance gradually rises during the dry season as the groundwater contribution proportionally increases, and then quickly decreases as a result of dilution from precipitation and runoff during the wet season. The rapid pressurization of the karst aquifer by low-mineral winter recharge and captured streamflow causes the release of proportionally more high-mineral groundwater to SP-1 Spring. The rise in spring flow specific conductance usually peaks one-half to three days after a storm begins. This observation demonstrates that a large volume of dynamic groundwater storage exists and contributes substantially during periods of both high and low discharge.

The mean daily specific conductance and water temperature of SP-1 Spring are directly correlated (Fig. 9.22e). Flows with the lowest specific conductance (<400 μS/cm) are coldest (<15 °C) whereas flows with the highest specific conductance (>450 μS/cm) are warmest (>16 °C). Cold temperatures and relatively low mineral content reflect captured winter streamflow, whereas relatively warm water (approaching mean-annual air temperature) and higher mineral content reflect long-term groundwater storage. SP-1 Spring's discharge of relatively warm, mineralized water during peak flow conditions indicates a direct and substantial contribution from groundwater storage.

9.6.2.2 Relationship Between Spring Discharge and Turbidity

The mean daily turbidity correlates poorly with mean daily flow (Fig. 9.22b). For example, turbidities > 10 Nephelometric Turbidity Unit (NTU) have occurred on days with mean daily flows anywhere between 900 and 3,000 gpm (Fig. 9.22b.). The lower limit of the turbidity-versus-flow envelope generally increases with increasing flow. However, the highest recorded turbidities have not occurred at the highest flows, but instead are most associated with flows between 900 and 2000 gpm. In streams, turbidity is more highly correlated with flow, including maximum flows. SP-1 Spring turbidities are slightly better correlated with specific conductance (Fig. 9.22c). The poor correlation between SP-1 Spring peak flows and peak turbidities indicates that peak turbidities tend to occur early during the spring's stormflow hydrograph.

Springs with a small watershed may show a direct correlation between discharge and turbidity. For springs with large watersheds such as SP-1 Spring, a direct correlation between discharge and turbidity does not usually exist for two reasons—the phase difference between the discharge hydrograph and the turbidigraph and a phenomenon called turbidity hysteresis. The lack of a relationship between discharge and turbidity is characteristic of many large karst springs (Valdes et al. 2005; Fournie et al. 2007).

Figure 9.23 shows a clockwise or positive loop of the hysteresis curves for a storm event. This loop generally occurs during an increase of water discharge, which is indicative of sediment resuspension by pressure transfer. The shape of these hysteresis curves varies significantly between storms, suggesting that the complex relationship between discharge and turbidity can be further complicated by the antecedent groundwater flow conditions and the characteristics of each rainfall.

Clearly, the turbidity is not directly correlated to the spring flow. The discharge hydrographs are normally distributed over a much longer time scale than the suspended sediment response. The peak concentration of suspended solids tends to precede peak spring flow and have a much shorter duration, a relationship that has been observed in other karst springs (Mahler and Lynch 1999; Townsend and Macfarlane 2003).

Hysteresis curves are often used to describe sediment transport in surface streams (Ongley 1996). Recently, they have been used to describe the characteristics of suspended solids at karst springs (Valdes et al. 2005; Fournie et al. 2007). The following explain the occurrence of turbidity hysteresis at SP-1 Spring:

- The most intensive transport processes in the system occur during the pressure transfer caused by a flood pulse. The flood pulse causes a highly unsteady flow regime, which causes resuspension and transport of deposited sediments. The increased intensity in the rising limb is caused by the flood pulse overtaking the baseflow. It has been demonstrated that turbulence intensities are generally larger in the rising limb of a hydrograph than in the falling limb, and the turbulence intensity becomes larger as the unsteadiness of the hydrograph in-creases (Sutter and Verhoeven 2001). These findings suggest strongly that sediment transport is the strongest in the rising stage when the flow is the most unsteady. It is the flow velocity and the acceleration of the flow that provide the turbulent intensity to resuspend the particles in the water.
- Rapid depletion of sediments that can be resuspended occurs for the storm events. The most mobile sediments are those recently deposited. Compacted sediments, even of fine grain size, require stronger basal shear stresses to mobilize than uncompacted sediments. Larger storms are required to resuspend the compacted or larger sediments temporarily stored in the system. Thus, the turbidity does not increase as the discharge in-creases, once the more mobile sediments have been entrained.

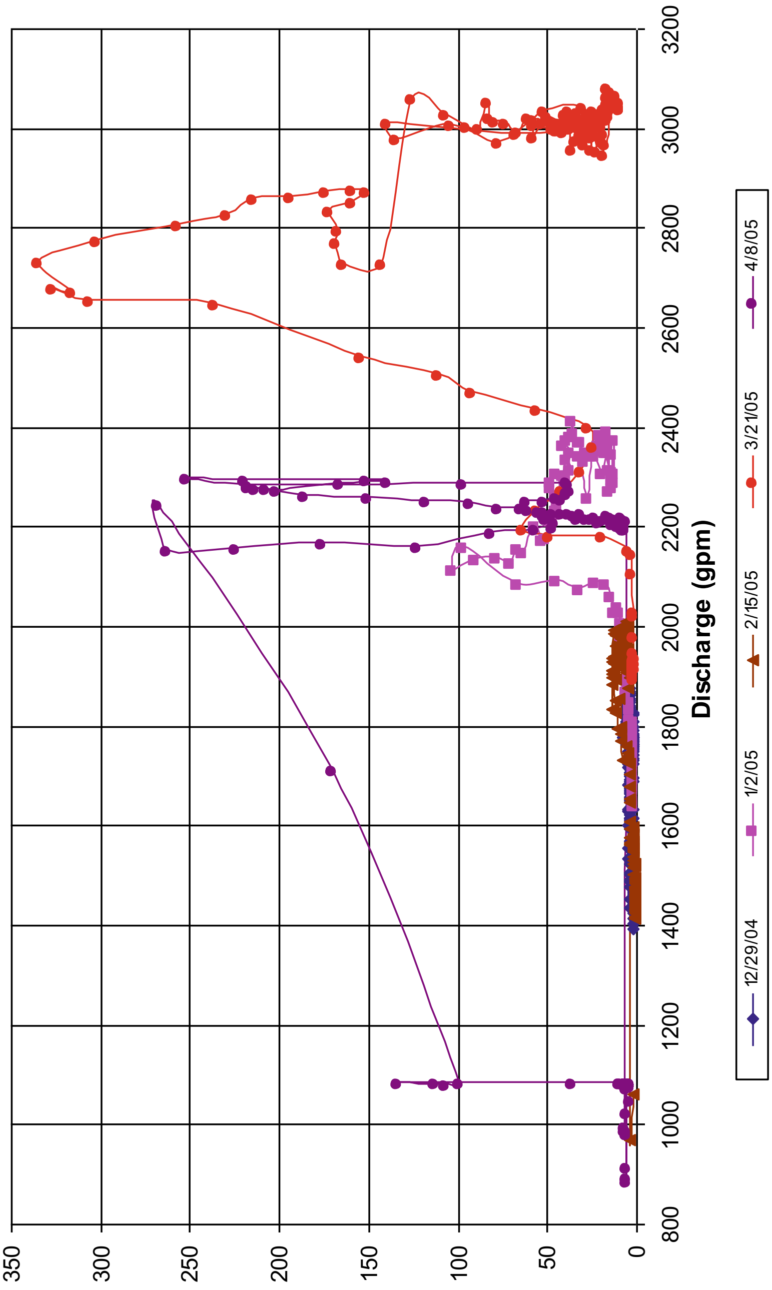

Fig. 9.23 Turbidity hysteresis at SP-1 spring for select storm events

9.6.3 Stable Isotopes

All groundwater has a “fingerprint” of naturally occurring isotopes that provides information about the origin of the water (Drever 1997). Waters that have the same sources tend to have similar isotopic signatures. Analysis of the stable isotopic ratios was designed to determine which waters have a similar isotopic signature to that at SP-1 Spring. A stable isotope survey was conducted at 39 quarry-area wells, springs, seeps, and streams in February 2003. Accumulated precipitation was 20 inches for the season to date, greater than 2 inches during the preceding 10 days, and about 1 inch during the sampling period.

Concentrations of the heavier isotopes of hydrogen and oxygen become depleted in water derived from evaporation. Thus, atmospheric moisture is depleted of the heavier isotopes relative to the ocean from which it evaporated. The isotopic composition of precipitation is further affected by the temperature and elevation of where it forms and falls. When precipitation accumulates on land, it becomes relatively enriched with the heavier isotopes as the lighter isotopes are disproportionately lost to evaporation. Once water percolates below ground it experiences no further evaporation and its isotopic ratios of hydrogen and oxygen remain fairly constant. Thus, groundwater at different locations, depths, and points of discharge can be grouped into similar origins and flow paths based on the similarity of these ratios, although various chemical processes can further alter the isotope ratios below ground. Figure 9.24 is a plot of the ratios of oxygen-18 to oxygen-16 ($\delta^{18}O$) versus the ratios of deuterium to hydrogen (δD). The corresponding values of specific conductance are posted beside each point. The isotope-ratio pairs are grouped within five separate envelopes based on their ratio values, specific conductance, and contextual hydrogeology.

- Group 1 consists of springs and seeps emerging from the Santa Margarita Sandstone (-5.4 to -5.8 $\delta^{18}O$, -32 to -34 δD). These have very low specific conductance values of less than 200 μS/cm. The envelope encompassing group 2 (-5.6 to -5.7 $\delta^{18}O$, -33 to -34 δD) nearly overlies group 1, however these samples are from monitoring wells completed in marble and have moderate to high values of specific conductance (350–900 μS/cm). The isotopic similarity of these groups, along with hydrogeologic interpretation, suggests that group 1 groundwater represents the source of group 2 groundwater, i.e., water recharged into the Santa Margarita Sandstone eventually migrates into the underlying marble aquifer.
- Group 3 consists of streamflow in the sinking streams SS-8 and SS-1 watersheds (-5.7 to -6.2 $\delta^{18}O$, -34 to -37 δD). Given the time of year, very low specific conductance, and approximately 3 inches of precipitation immediately prior to and during the survey, these samples are probably more representative of seasonal runoff than baseflow. Stream samples taken at other times would probably have substantially different isotopic signatures. However, these samples do represent the seasonal flows most available for capture by the karst sinkholes.
- Group 4 (-5.7 to -6.0 $\delta^{18}O$, -34 to -35 δD) consists of groundwater with moderately low specific conductance (~200–400 μS/cm) from relatively deep monitoring wells located along major fracture zones. This group overlies one end

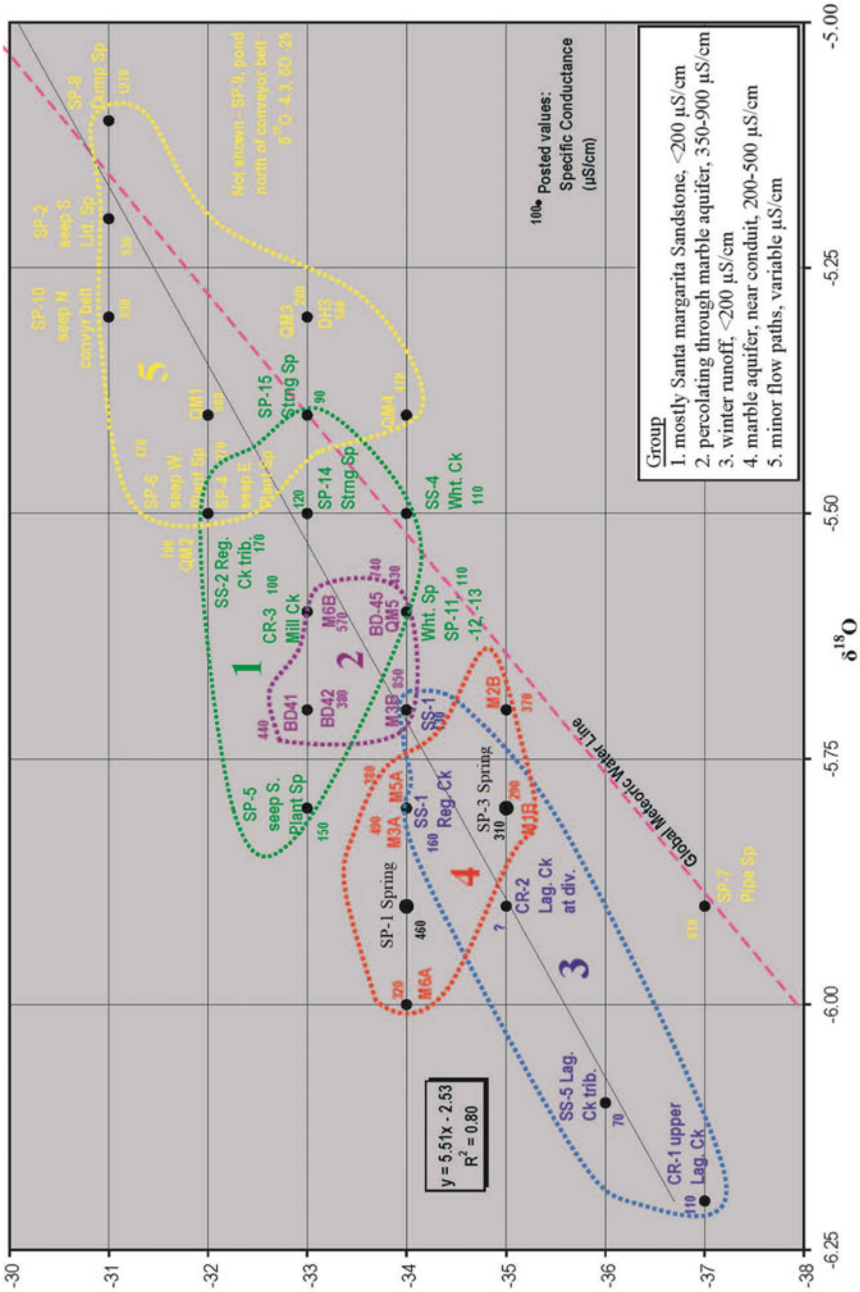

Fig. 9.24 Results of stable isotopes

of the group-3 envelope, consistent with the assumption that this groundwater is recharged predominantly by stream swallow holes. This group probably receives some leakage from shallower zones, thus explaining its location toward groups 1 and 2 relative to the center of group 3. Also, the rapid arrival of tracers to SP-1 Spring suggests that none of these monitoring wells directly encounter the highest permeability pathways.

- SP-1 Spring (-5.9 δ^{18}O, -34 δD) plots midway between groups 1–2 and groups 3–4 in terms of δD, whereas in terms of δ^{18}O the spring plots approximately midway between groups 1–2 and the more depleted (i.e., more negative) portion of group 3. These data indicate that both sandstone recharge and sinkhole stream capture contribute roughly equally to the spring. The fact that the spring's δ^{18}O is skewed toward the depleted end of group 3 is reasonable given that the greatest volume of sinking recharge is from isotopically depleted stormflow. SP-3 Spring (-5.8 δ^{18}O, -35 δD) plots within group 4 in terms of both δD and δ^{18}O. This and its moderately low specific conductance suggest that its source is mostly from captured streamflow.
- Group 5 is isotopically enriched relative to the other groups (-5.1 to -5.5 δ^{18}O, -31 to -34 δD, except for two outliers). This group includes all the non-calcium-bicarbonate waters, including those that appear influenced by quarry waste and/or migrate along fairly minor flow paths separate from the karst groundwater system (i.e. conceptual path *D*). This group partially overlies group 1 but is distinguished by generally higher values of specific conductance. A sample of highly enriched pond water (SS-9) suggests that the water had resided in the pond for an extended period of time and experienced considerable evaporation.

9.7 Turbidity and Sediment

9.7.1 Transport and Sources of Sediments in SP-1 Spring

Non-karstic aquifers do not often carry a sediment load because the pores through which the water flows are too small, and the flow velocities are too slow for sediment transport. The porous medium acts as an effective filter, allowing infiltrating groundwater to pass but rejecting solid material, which is left on the surface as a weathered residuum. Unlike a porous medium aquifer, a karst aquifer is characterized by enhanced permeability that permits high flow velocities capable of transporting suspended and bedload sediments. Calculations have shown that the transport of suspended sediments can occur in fracture openings as small as 1 cm (White 1988). Consideration of the critical boundary shear for bedload transport shows that flow velocities in the range of fractions of a meter per second are required to set the sediments into motion. Quantitative studies of sediment transport in conduits are sparse, but anecdotal evidence indicates that most sediment moves during flood events (White 1993). Extreme flood flows may strip a conduit system of its sediment filling. New material is deposited during flood recessions as in surface channels after floods.

Both SP-1 Spring and SP-3 Spring are karst springs. Although the flow paths to SP-3 Spring are different from those to SP-1 Spring, its water has turbidity spikes in response to precipitation events. The discussion of turbidity in SP-1 Spring and its close association with rainfall events dates back at least to 1956 (Todd 1963). Historic documents reporting turbidity spikes in response to rainfall events indicate a wide range in the turbidity levels for storms of similar magnitudes. Because of the complicated processes of sediment transport in the karst aquifer, the magnitudes of the turbidity response and the lag time vary significantly from one storm to another.

Like in any other well-developed karst aquifer, the transport of sediments is episodic and is very sensitive to the flow regime. The most significant sediment transport occurs primarily during storm flow and the rate of transport can vary greatly over the year, depending on storm intensity and overall flow rates. As storm flow recedes, the sediments are deposited in the conduit system and at the spring mouths. Both depositional and erosional processes occur in the conduits. Storm flow provides a means of flushing out the accumulated materials at springs. The presence of mobile sediments in karst has been recognized for several decades (Bretz 1964). It is well documented that water quality at karst springs can be impacted due to the increase in turbidity during storm events (Atteia and Kozel 1997; McCarthy and Schevenell 1998; Schevenell and McCarthy 2002; Mahler and Lynch 1999). Transport of sediment particles is an essential part of the functioning of the karst aquifer. In well-developed aquifers where surface streams sink underground, the insoluble materials carried by the sinking surface streams are carried through the conduit system and washed out through the springs. If this did not happen, the conduit system would eventually become clogged with sediment and drainage would be forced to the surface. A karst aquifer only continues to function if the flow is sufficient to transport the sediment and prevent clogging.

Similar to the water recharge sources for SP-1 Spring, the sediment sources can also be divided into allogenic and autogenic categories. Weathered products from the erosion of the borderland enter the aquifer through the sinking streams and the Sinkhole Plain. When these streams flow underground through the karst, so do the sediments. Carbonate rocks also contain a small percentage of insoluble material, and these materials accumulate as soils on the karst surface and as weathered residuum created in the subsurface by the solutional enlargement of the conduit system. According to the results from the tracing tests and the local geology, the following sources may provide natural sediments to SP-1 Spring.

- Sinkholes.
- Sinking streams SS-1, SS-2, SS-4, and SS-8.
- Landslide adjacent to SP-1 Spring.
- Weathered residuum on the surface and in the subsurface in the karst land.
- Quarry floor.

This study indicates that the sinkhole plain and sinking stream SS-1 are probably the most important sources supplying the sediments into the karst system. The sinkhole plain is active and sandy sediments are present. The runoff from the local springs or from rainfall can carry significant amount of sediments into the subsurface. At the sinking section of SS-1, sediments can be observed being transported into the subsurface through fractures in the marble. Small funnel-shaped depressions are present in the unconsolidated materials along the western riverbank, indicating downward transport of the sediments. The sediments can be stored in the conduit/fractures system temporarily and their further transport relies on the intensity of rainfall. Similar sediments have been observed in caves and some of the boreholes.

Sinking stream SS-8 is well connected to SP-1 Spring and can provide sediments to the karst system. Because the sinking section of SS-8 is approximately 2.7 miles away from SP-1 Spring, its contribution of sediments to SP-1 Spring is not instantaneous.

Because the spring box at SP-1 Spring receives water from the marble and the landslide deposits, a flow regime change in the deposits may move sediments in the slide deposits into the spring box. A local flow regime change can also mobilize the sediments that are stored at the spring mouth.

Because of the poor hydraulic connection between the unsaturated zone and the saturated zone, the sediment contribution from the autogenic source is limited. It is important to realize that most of the autogenic sediments are from natural dissolution processes, regardless of the existence of the quarry.

The autogenic source also includes the particulates present on the quarry floor. The sediments on the quarry floor may contribute to the turbidity at SP-1 Spring only if open fractures are present and when water flow carries the sediments into the subsurface. When no open fractures are present, the marble block is not permeable to sediments. The sediments on the existing quarry floor are angular and poorly sorted, whereas the sediments discharged at SP-1 Spring are rounded and well sorted. The X-ray diffraction analysis of suspended sediment samples at SP-1 Spring reported the average composition of the sediments: 32.7% quartz, 28.7% feldspars, 3.7% mica, 10% calcite, 1.5% hematite, 20.8% clay, and 2.7% unaccounted materials. Because the sediments on the quarry floor are predominantly calcite, the mineralogical composition does not point to a single source.

9.7.1.1 Transport and Sources of Sediments in SP-1 Spring

Turbidity represents the cloudiness of water caused by the presence of fine suspended matter. It can be measured by the presence of total suspended solids in water, which is reported in parts per million (ppm), or determined by measurements of light diffraction, which is reported in NTU. According to the National Primary Drinking Water Regulations (www.epa.gov/safewater), a Maximum Contaminant Level Goal is not established for turbidity. The Maximum Contaminant Level for turbidity value is 5 NTU. Turbidity has no health effects but can interfere with disinfection and provide a medium for microbial growth.

Elevated turbidity is a main concern at SP-1 Spring because it is a water supply source. Figure 9.25 shows the base-level turbidity data at SP-1 Spring from 1960 to 2004. The base level is defined a condition when no rainfall occurred during the month. These data demonstrate the turbidity variation when the precipitation impacts are excluded. A quality control chart is developed to demonstrate that no long-term

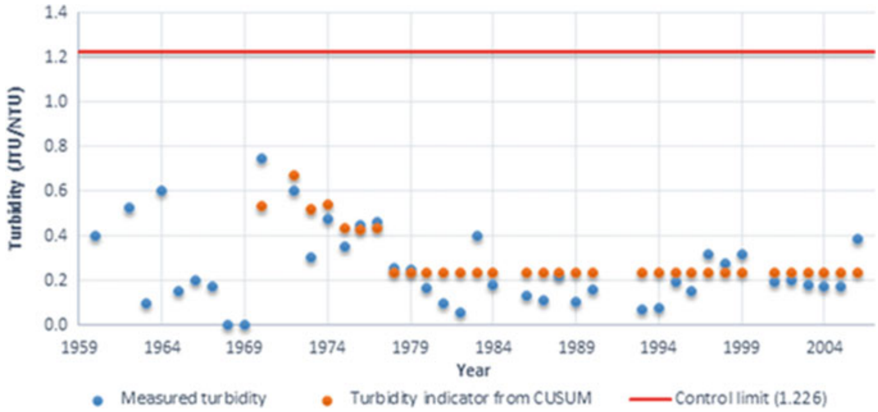

Fig. 9.25 Long-term base-level turbidity changes

degradation of base-level water quality due to turbidity. The pre-quarry samples collected from 1960 to 1969 are used to estimate the control limits.

Quality control chart method is a viable way to analyze the dataset to statistically determine if the quarry operations have changed the turbidity levels at SP-1 Spring. Because quarry operations may cause both large and small changes in the turbidity values, the Combined Shewhart-CUSUM control charts are used in the analysis. Combined Shewhart-CUSUM control charts are the statistical procedures directly recommended by U.S. EPA (1989,1992) and American Society for Testing and Materials (ASTM) (1998). As implied by its name, a combined Shewhart-CUSUM control chart is a mixture of two statistical schemes: Shewhart control scheme and CUSUM control scheme. The Shewhart control scheme is better in quickly detecting a large shift in the mean; whereas, the CUSUM scheme is usually faster in detecting a small change in the mean that persists.

Design of a combined control chart requires the determination of the following five parameters:

$\overline{X}$ Estimated mean of turbidity from pre-quarry samples from 1960 to 1969. The calculated annual average mean is 0.269 NTU.

S Estimated standard deviation of turbidity from pre-quarry samples from 1960 to 1969. The calculated standard deviation is 0.214 NTU.

h The value against which the cumulative sum will be compared.

k A parameter related to the displacement that should be quickly detected.

SCL The upper Shewhart limit, which is the number of standard deviation units for an immediate release.

For turbidity measurement x_i after the quarry began its operations, the standardized difference z_i is calculated by (EPA 1989):

$$z_i = \frac{x_i - \overline{X}}{S}$$

And, the cumulative sum Y_i is calculated by:

$$Y_i = \max\left[0, (z_i - k) + Y_{i-1}\right]$$

A significant turbidity change is declared when either $Y_i \geq h$ or $z_i \geq SCL$. EPA (1989) recommends using SCL = 4.5, k = 1, and h = 5 to allow a displacement of two standard deviations to be detected quickly (EPA 1992). For easy application, ASTM (1998) suggested the use of h = SCL = 4.5, which is slightly more robust in detecting any turbidity changes. For this application, we use h = SCL = 4.5.

The red horizontal line in Fig. 9.25 is the control limit. The control chart suggests that there are no statistically significant changes in turbidity due to quarry operations.

9.8 Statistical Analysis of Turbidity Responses to Quarry Blasting

Blasting is used to break-up the rock using ammonium nitrate as part of the operations at the quarry. Thirty to fifty-foot holes are drilled on a working bench and the charge is set in the blast holes. When an explosive is detonated, most of the energy from a properly designed blast works to displace rock from the quarry face. The remaining energy is released as vibrations through and along the surface of the earth and through the air. The blast-induced vibrations have been monitored as ground acceleration at various locations in the quarry and in its vicinity. The correlation between quarry blasting and turbidity spikes at SP-1 Spring is statistically analyzed to provide a detailed quantitative study on the possible impacts of quarry blasting on the turbidity at SP-1 Spring in combination with rainfall and antecedent soil conditions.

9.8.1 Data Collection and Validation

Valid statistical analysis relies on the availability and validity of the data to be analyzed. The purpose of this statistical analysis requires careful validation of three sets of data—blasting data in the quarry, precipitation data in the local area, and turbidity data at SP-1 Spring. Although precipitation and turbidity data are available for over decades, only those collected during the periods when the quarry blasting was monitored were analyzed during this study. Figure 9.26 shows one-month data as an example of data available for the analysis.

Because the data were collected by various organizations, different techniques, and different frequencies, professional judgment was applied to validation of the data. Figure 9.27 shows the general data selection processes. The precipitation data and turbidity data were converted to hourly intervals for the statistical analysis. The hourly turbidity is the average value if more than one reading is available within one hour, whereas the hourly precipitation is the cumulative value within each hour.

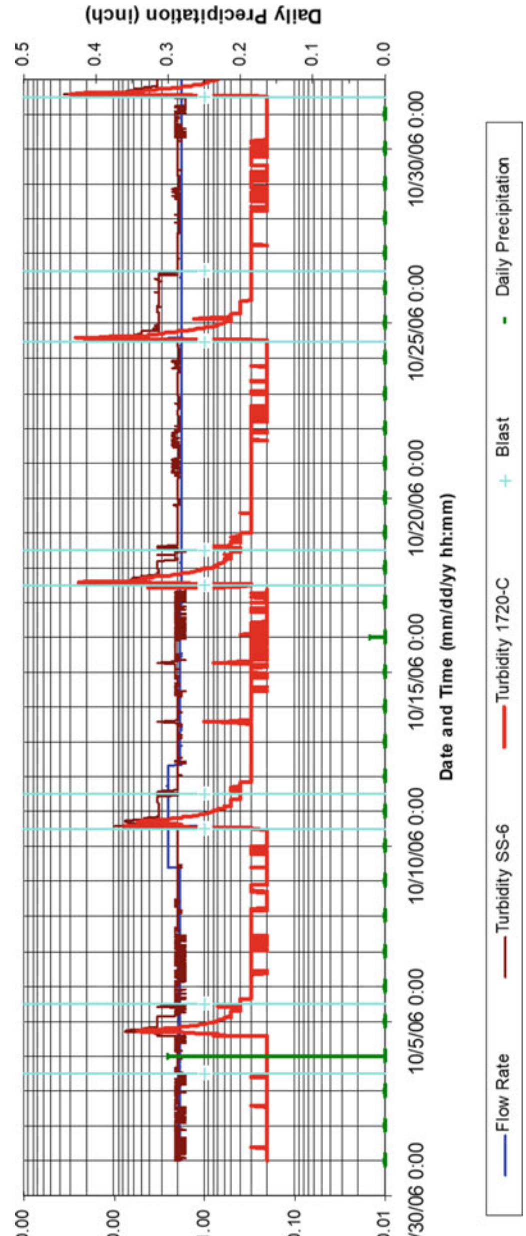

Fig. 9.26 Example of data available for statistical analyses

Fig. 9.27 Flowchart for blasting and turbidity data selection

Table 9.8 Blasting events used for statistical analysis for each scenario

		Precipitation 1 day prior to blasting		Precipitation 5 days prior to blasting		Precipitation 30 days prior to blasting	
		No	Yes	No	Yes	No	Yes
Precipitation 24 h After Blasting	No	57	18	34	51	4	98
	Yes	10	9	1	18	0	19

From November 1997 to June 2004, 335 blasting events were recorded in the quarry. Of these, 173 blasting events did not have corresponding turbidity data. The availability of precipitation data and the validation processes further eliminated 32 events. Therefore, 130 events were considered to consist of valid data, and they were used for the current study. Based on the precipitation data prior to and after each blast, the blast events were further divided into different categories. 111 blasting events occurred when there was no precipitation within 24 h after the blasting, while 19 events occurred when there were precipitation activities within 24 h after the blasting.

The antecedent soil moisture condition was considered by the cumulative precipitation activities prior to each blasting event. The precipitation 1 day, 5 days, and 30 days prior to the blasting event was considered. Table 9.8 provides 12 scenarios in which the statistical analyses are performed, and the number of events used for the respective analysis.

From a statistical perspective, reliable results rely on a large number of blasting events. When there is only one blasting event, such as the scenario in which there were precipitation activities within 24 h after the blasting but there was no precipitation 5 days prior to the blasting event, the results cannot be statistically analyzed. Because none of the blasting events occurred when there was a precipitation activity within 24 h after the blast, but there was no precipitation 30-days prior to the blast, no statistical analysis can be performed for this scenario either. The first measured turbidity change at SP-1 Spring tends to occur within a few hours; therefore, the turbidity values measured within 24 h after each blasting event were used for the analysis.

9.8.2 Statistical Analysis

The main challenge in the statistical analysis is to separate the impact of blasting from the impact of precipitation. When precipitation occurs prior to blasting, the water at SP-1 Spring is already affected by the rainfall, which will overshadow the possible impact of blasting. When precipitation occurs after blasting, the impact from the blasting is masked by the impact from precipitation. In addition, the turbidity at

SP-1 Spring is affected by other factors, such as activities in the catchment basin areas and the transport characteristics of the solid particles in the marble aquifer.

To evaluate the impact of blasting on turbidity at SP-1 Spring, the turbidity values within 24 h after the blasting were compared with the hourly average turbidity one-hour prior to blasting. The turbidity change was calculated for each of the 24 h after each blasting event by subtracting the hourly turbidity value one-hour prior to blasting from the hourly turbidity values after blasting. The turbidity change was used for the statistical analysis.

Statistically, the turbidity change would be zero or close to zero if the blasting has no impact on the turbidity at SP-1 Spring, provided that the impact of precipitation can be eliminated. It can also be reasonably assumed that the turbidity change would be greater than zero if the blasting has an impact on the turbidity at the spring. The magnitude of the turbidity change indicates the extent to which the blasting affects the turbidity at SP-1 Spring. Because none of the blasting events occurred when there was precipitation activity 24 h after the blasting but there was no precipitation 30-day prior to the blasting and only one blasting event is available for the scenario in which there were precipitation activities within 24 h after the blasting but no precipitation activities 5 days prior to the blasting event, only 10 scenarios of the 12 listed in Table 9.8 were actually analyzed.

Table 9.9 provides the analysis results. For each scenario, the average, median, mode, minimum, maximum, and standard deviation of the turbidity change were calculated for each of the 24 h after the blasting. Because the turbidity data were collected by different organizations and different sensors, the turbidity values may not be absolutely comparable throughout the monitoring period and the average value is probably the most representative of the turbidity change. Table 9.10 lists the main characteristics of the average turbidity change for the 10 scenarios analyzed. The data for the scenario in which only one blasting event is available are also presented in the table, although they do not have statistical meaning.

9.8.3 Impact of Blasting on Turbidity at SP-1 Spring

The impact of blasting on the turbidity at SP-1 Spring can only be evaluated when the effects of other factors can be precluded, i.e., when the impact of precipitation on the turbidity at SP-1 Spring is minimal prior to and after blasting. The scenario in which there was no precipitation 30 days prior to blasting and no precipitation within 24 h after blasting, may best fit this criterion. The average hourly turbidity prior to blasting is 1.44 NTU, which may represent the background value when SP-1 Spring is not affected by either precipitation or blasting. As shown in Table 9.10, the turbidity change has a positive response in the first hour after blasting and the response lasts approximately 18 h. The magnitude of the response is less than 0.5 NTU, with a range from 0.03 to 0.33 NTU. The maximum response occurs 5–6 h after blasting. For any particular blasting event, the turbidity change could be up to 1.27 NTU, which also occurred 5–6 h after blasting.

Table 9.9 Results of statistical analysis

Scenarios	Time after blast (h)	Statistical results					
		Average (NTU)	Median (NTU)	Mode (NTU)	Minimum (NTU)	Maximum (NTU)	Standard deviation
• No precipitation within 24 h after blasting • No precipitation 1 day prior to blasting • Number of Blasting Event: 57	0–1	0.11	0.02	0	−0.35	2.03	0.36
	1–2	0.36	0.05	0	−0.55	5.17	0.96
	2–3	1.3	0.1	0	−0.6	36.62	5.05
	3–4	0.84	0.1	0	−2.7	7.45	1.84
	4–5	1	0.15	0	−2.86	16.19	2.47
	5–6	1.5	0.15	0	−2.7	35.04	5.29
	6–7	1.27	0.1	0	−2.7	24.48	4.46
	7–8	1.09	0.1	0	−3.01	27.22	4.1
	8–9	0.74	0.08	0	−3.01	15.82	2.57
	9–10	0.54	0.08	0	−2.86	9.89	1.72
	10–11	0.37	0.08	0	−2.7	6.69	1.24
	11–12	0.28	0.08	0	−2.7	5.17	1.03
	12–13	0.22	0.05	0	−2.7	4.57	0.88
	13–14	0.2	0.02	0	−1.43	3.96	0.75
	14–15	0.14	0	0	−2.7	3.35	0.72
	15–16	0.12	0	0	−2.86	2.74	0.67
	16–17	0.11	0	0	−2.7	2.74	0.67
	17–18	0.1	0	0	−2.7	2.74	0.69
	18–19	0.07	−0.02	0	−2.7	3.42	0.77
	19–20	0.09	0	0	−2.7	2.74	0.69
	20–21	0.06	−0.03	0	−2.7	2.25	0.65
	21–22	0.07	−0.05	0	−2.7	2.58	0.71
	22–23	−0.04	0	0	−2.86	2.08	0.66
	23–24	−0.07	0	0	−3.78	2	0.72
• No precipitation within 24 h after blasting • With precipitation 1 day prior to blasting • Number of Blasting Event: 18	0–1	0.15	0	0	−35.91	48	14.9
	1–2	−2.95	0	0	−38.74	0.63	9.25
	2–3	−1.95	0.16	0.16	−43.16	5	10.5
	3–4	−2.49	0.74		−42.91	3.94	10.62
	4–5	−2.84	0.25	0.05	−42.24	4.13	10.63
	5–6	−3.22	0.14	0	−41.66	6.56	11.32
	6–7	−3.66	0.1	0	−41.91	3.04	11.26
	7–8	−3.94	0.13	1.37	−41.99	2.73	11.26
	8–9	−4.16	0.08		−41.83	2.05	11.3
	9–10	−4.18	0.09	0	−40.91	1.52	11.11
	10–11	−4.32	0.06	0	−40.74	1.52	11.13
	11–12	−4.37	0.03	0	−40.58	1.37	11.09

(continued)

Table 9.9 (continued)

Scenarios	Time after blast (h)	Statistical results					
		Average (NTU)	Median (NTU)	Mode (NTU)	Minimum (NTU)	Maximum (NTU)	Standard deviation
	12–13	−4.61	0	0	−39.99	1.44	11.37
	13–14	−4.58	0	0	−39.41	1.15	11.08
	14–15	−4.72	−0.02	−0.02	−39.08	0.88	10.93
	15–16	−4.74	−0.01	0	−39.66	0.9	11.08
	16–17	−4.8	−0.05	0	−39.91	0.45	11.06
	17–18	−4.79	−0.08	0	−39.08	0.7	10.89
	18–19	−4.88	−0.08	0	−40.16	0.08	11.11
	19–20	−4.92	−0.08	0	−40.91	0.88	11.3
	20–21	−4.98	−0.16	−0.08	−40.66	1.25	11.34
	21–22	−4.57	−0.1	0	−40.33	0.53	11.24
	22–23	−4.82	−0.13	0	−40.91	0.08	11.43
	23–24	−4.16	−0.1	0	−40.33	0.13	10.13
• No precipitation within 24 h after blasting • No precipitation 5 days prior to blasting • Number of Blasting Event: 34	0–1	0.08	0.03	0	−0.35	0.8	0.22
	1–2	0.18	0.07	0	−0.55	1.37	0.37
	2–3	0.28	0.09	0	−0.6	1.5	0.51
	3–4	0.53	0.08	0.08	−0.53	5.78	1.12
	4–5	0.86	0.09	0	−0.55	16.19	2.78
	5–6	1.39	0.09	0	−0.6	35.04	5.97
	6–7	0.91	0.1	0	−0.63	23.41	4
	7–8	0.58	0.03	0	−0.55	14.82	2.55
	8–9	0.47	0.05	0	−0.48	10.79	1.86
	9–10	0.38	0.06	0	−0.58	7.45	1.32
	10–11	0.26	0.04	0	−0.65	5.17	0.93
	11–12	0.17	0.05	0.13	−0.65	4.25	0.77
	12–13	0.15	0.03	0	−0.48	2.81	0.55
	13–14	0.11	0	0	−0.5	2.73	0.52
	14–15	0.08	0	0	−0.55	1.9	0.41
	15–16	0.08	0	0	−0.43	1.52	0.35
	16–17	0.05	0	0	−0.65	1.52	0.38
	17–18	0.03	0	0	−0.5	1.52	0.32
	18–19	−0.03	−0.03	0	−0.88	1.52	0.35
	19–20	0.03	0	0	−0.48	1.52	0.35
	20–21	0	−0.03	0	−0.53	1.52	0.32
	21–22	0.09	−0.03	0	−0.55	2.58	0.55
	22–23	−0.06	0	0	−2.18	1.52	0.49
	23–24	−0.1	0	0	−3.78	0.84	0.7

(continued)

Table 9.9 (continued)

Scenarios	Time after blast (h)	Statistical results					
		Average (NTU)	Median (NTU)	Mode (NTU)	Minimum (NTU)	Maximum (NTU)	Standard deviation
• No precipitation within 24 h after blasting • With precipitation 5 days prior to blasting • Number of Blasting Event: 51	0–1	0.15	0	0	−35.91	48	8.7
	1–2	−0.78	0.02	0	−38.74	5.17	5.72
	2–3	0.62	0.16	0	−43.16	36.62	8.3
	3–4	−0.28	0.16	0	−42.91	7.45	6.67
	4–5	−0.28	0.16	0	−42.24	7.63	6.7
	5–6	−0.03	0.23	0	−41.66	19.92	7.68
	6–7	−0.22	0.16	0	−41.91	24.48	7.93
	7–8	−0.37	0.2	0.13	−41.99	27.22	8.06
	8–9	−0.84	0.16	0	−41.83	15.82	7.42
	9–10	−1.03	0.1	0	−40.91	9.89	7.06
	10–11	−1.2	0.1	0	−40.74	6.69	6.99
	11–12	−1.3	0.02	0	−40.58	5.17	6.94
	12–13	−1.45	0	0	−39.99	4.57	7.1
	13–14	−1.42	0.02	0	−39.41	3.96	6.93
	14–15	−1.59	0	0	−39.08	3.35	6.85
	15–16	−1.67	0	0	−39.66	2.74	6.91
	16–17	−1.61	0	0	−39.91	2.74	6.9
	17–18	−1.66	−0.02	0	−39.08	2.74	6.81
	18–19	−1.71	−0.05	0	−40.16	3.42	6.96
	19–20	−1.63	0	0	−40.91	2.74	7.07
	20–21	−1.78	−0.08	0	−40.66	2.25	7.08
	21–22	−1.69	−0.08	0	−40.33	2.25	6.94
	22–23	−1.72	0	0	−40.91	2.08	7.09
	23–24	−1.51	−0.05	0	−40.33	2	6.25
• No precipitation within 24 h after blasting • No precipitation 30 days prior to blasting • Number of Blasting Event: 4	0–1	0.03	0	0	−0.19	0.31	0.21
	1–2	0.16	0.16		0	0.31	0.15
	2–3	0.09	0.16		−0.31	0.38	0.32
	3–4	0.09	0.06		−0.06	0.31	0.16
	4–5	0.11	0.16		−0.19	0.31	0.25
	5–6	0.33	0.28		−0.5	1.27	0.73
	6–7	0.22	0.22		−0.19	0.64	0.34
	7–8	0.11	0.16		−0.25	0.38	0.29
	8–9	0.09	0.13		−0.19	0.31	0.23
	9–10	0.12	0.13		−0.06	0.31	0.18

(continued)

Table 9.9 (continued)

Scenarios	Time after blast (h)	Statistical results					
		Average (NTU)	Median (NTU)	Mode (NTU)	Minimum (NTU)	Maximum (NTU)	Standard deviation
	10–11	0.05	0.06		−0.06	0.16	0.1
	11–12	0.04	0		−0.16	0.31	0.22
	12–13	0.11	0.16		−0.19	0.31	0.25
	13–14	0.08	0.13		−0.25	0.31	0.26
	14–15	0.14	0.16		−0.13	0.38	0.24
	15–16	0.1	0.12		−0.16	0.31	0.25
	16–17	0.03	0.13		−0.44	0.31	0.34
	17–18	0.03	0.06		−0.31	0.31	0.26
	18–19	−0.22	−0.16		−0.88	0.31	0.51
	19–20	0.02	0	0	−0.16	0.25	0.17
	20–21	0.17	0.16	0	0	0.38	0.2
	21–22	0.12	0.08		−0.06	0.38	0.19
	22–23	0.03	0	0	−0.25	0.38	0.26
	23–24	−0.02	0.09		−0.56	0.31	0.39
• No precipitation within 24 h after blasting • With precipitation data points 30 days prior to blasting • Number of Blasting Event: 98	0–1	0.08	0	0	−35.91	48	6.25
	1–2	−0.34	0.03	0	−38.74	5.17	4.16
	2–3	0.8	0.08	0	−43.16	36.62	6.79
	3–4	0.88	0.1	0.05	−42.91	72.19	8.79
	4–5	0.58	0.1	0	−42.24	32.31	6.13
	5–6	0.81	0.11	0	−41.66	35.04	7.29
	6–7	0.44	0.09	0	−41.91	24.48	6.43
	7–8	0.25	0.06	0	−41.99	27.22	6.32
	8–9	−0.1	0.06	0	−41.83	15.82	5.67
	9–10	−0.23	0.06	0	−40.91	15.25	5.41
	10–11	−0.37	0.07	0	−40.74	12.69	5.28
	11–12	−0.62	0	0	−40.58	5.17	5.06
	12–13	−0.62	0.02	0	−39.99	5.94	5.22
	13–14	−0.69	0	0	−39.41	3.96	5.05
	14–15	−0.74	0	0	−39.08	7.19	5.06
	15–16	−0.82	0	0	−39.66	4.88	5.07
	16–17	−0.77	0	0	−39.91	3.88	5.06
	17–18	−0.54	−0.01	0	−39.08	30.41	5.89
	18–19	−0.86	−0.03	0	−40.16	4.06	5.1
	19–20	−0.84	0	0	−40.91	3.75	5.17

(continued)

Table 9.9 (continued)

Scenarios	Time after blast (h)	Statistical results					
		Average (NTU)	Median (NTU)	Mode (NTU)	Minimum (NTU)	Maximum (NTU)	Standard deviation
	20–21	−0.95	−0.06	0	−40.66	3.69	5.18
	21–22	−0.88	−0.06	0	−40.33	2.75	5.1
	22–23	−0.95	−0.03	0	−40.91	2.94	5.18
	23–24	−0.79	−0.03	0	−40.33	4.25	4.6
• With precipitation within 24 h after blasting • All precipitation data points prior to blasting or 30 days prior to blasting • Number of Blasting Event: 19	0–1	−0.78	0.08	0	−16.38	1.14	3.84
	1–2	−0.86	0.03	0	−16.7	7.61	5.05
	2–3	0.43	0.16	0	−16.6	8.7	4.68
	3–4	0.58	0.3	0	−16.63	7.52	4.88
	4–5	0.69	0.25		−16.65	9.65	5.04
	5–6	0.59	0.08	0	−16.55	10.34	5.18
	6–7	0.34	0.13	0	−16.58	11.4	5.39
	7–8	−0.12	0.05	0	−16.53	6.38	4.76
	8–9	−0.45	0	0	−16.78	4.41	4.48
	9–10	−0.71	0.1	0	−16.4	3.56	4.74
	10–11	−0.76	0.08	0	−16.48	3.19	4.39
	11–12	−0.91	0	0	−16.55	3.25	4.3
	12–13	−1.26	0	0	−16.5	3.56	5.16
	13–14	−0.9	0.05	0	−16.6	3.69	4.43
	14–15	−1.04	0.03	0	−16.48	3.44	4.62
	15–16	0.29	0	0	−16.68	28.63	8.19
	16–17	2.75	0	0	−16.7	79.44	19.12
	17–18	14.67	0	0	−16.6	306.75	70.88
	18–19	4.32	0	0	−16.6	94.38	22.68
	19–20	7.65	0	0	−16.7	107.03	29
	20–21	9.52	0	0.1	−16.7	150.2	36.84
	21–22	7.41	0.05	−0.08	−16.75	122.11	29.4
	22–23	4.17	0.03	0	−16.6	86.11	20.77
	23–24	3.84	0.08	0	−16.45	78.86	19.18
• With precipitation within 24 h after blasting • No precipitation 1 day prior to blasting • Number of Blasting Event: 10	0–1	−1.48	0.07	0	−16.38	0.61	5.24
	1–2	−0.77	0	0	−16.7	7.61	6.08
	2–3	0.1	0.34	0	−16.6	8.7	6.45
	3–4	0.33	0.93		−16.63	7.52	6.44
	4–5	0.75	0.82		−16.65	9.65	6.89
	5–6	0.47	0.23		−16.55	10.34	6.89
	6–7	−0.17	0.09		−16.58	7.98	6.33

(continued)

Table 9.9 (continued)

Scenarios	Time after blast (h)	Statistical results					
		Average (NTU)	Median (NTU)	Mode (NTU)	Minimum (NTU)	Maximum (NTU)	Standard deviation
	7–8	−0.47	0.01		−16.53	5.78	6.03
	8–9	−0.78	0	0	−16.78	4.41	5.87
	9–10	−0.85	0.08		−16.4	3.56	5.66
	10–11	−1.04	−0.01		−16.48	3.19	5.57
	11–12	−1.29	0	0	−16.55	3.25	5.51
	12–13	−1.29	0	0	−16.5	3.56	5.51
	13–14	−1.3	0.03	0	−16.6	3.69	5.55
	14–15	−1.34	0.01		−16.48	3.44	5.52
	15–16	1.19	0	0	−16.68	28.63	11
	16–17	6.11	0.01	0	−16.7	79.44	26.3
	17–18	28.83	−0.01	0	−16.6	306.75	97.79
	18–19	9.3	0	0	−16.6	94.38	30.87
	19–20	15.54	0	0	−16.7	107.03	39.01
	20–21	19.04	−0.03		−16.7	150.2	49.86
	21–22	14.74	−0.04	−0.08	−16.75	122.11	39.83
	22–23	8.8	0.01		−16.6	86.11	28.2
	23–24	8.11	0.04	0	−16.45	78.86	26.04
• With precipitation within 24 h after blasting • With precipitation 1 day prior to blasting • Number of Blasting Event: 9	0–1	−0.01	0.08	0.13	−2.5	1.14	1.04
	1–2	−0.96	0.08		−11.44	1.45	3.97
	2–3	0.79	0.08		−0.44	3.78	1.47
	3–4	0.85	0.08		−3	5.86	2.61
	4–5	0.63	0.15		−2.81	3.7	1.97
	5–6	0.73	0.05	0	−3.31	6.48	2.62
	6–7	0.9	0.13		−5.56	11.4	4.41
	7–8	0.26	0.05	0	−6	6.38	3.12
	8–9	−0.08	0.05	0	−6.06	3.13	2.48
	9–10	−0.55	0.13		−10.44	2.7	3.81
	10–11	−0.45	0.13		−7.94	1.65	2.86
	11–12	−0.5	0.06		−7.44	1.23	2.65
	12–13	−1.22	0.1		−14.63	1.55	5.07
	13–14	−0.47	0.15		−8.31	1.6	3.02
	14–15	−0.71	0.13		−10.31	1.55	3.66
	15–16	−0.71	0.1	0	−10.06	1.45	3.57
	16–17	−0.98	0	0	−11	1.53	3.8

(continued)

Table 9.9 (continued)

Scenarios	Time after blast (h)	Statistical results					
		Average (NTU)	Median (NTU)	Mode (NTU)	Minimum (NTU)	Maximum (NTU)	Standard deviation
	17–18	−1.06	0	0	−11.81	1.43	4.07
	18–19	−1.21	0.05		−12.94	1.58	4.43
	19–20	−1.12	0		−11.88	1.43	4.07
	20–21	−1.07	0.05		−11.94	1.55	4.12
	21–22	−0.74	0.13		−11.69	2.36	4.19
	22–23	−0.96	0.06		−12.69	1.48	4.44
	23–24	−0.91	0.08		−11.81	1.52	4.13
• With precipitation within 24 h after blasting • With precipitation 5 days prior to blasting • Number of Blasting Event: 18	0–1	−0.83	0.07	0	−16.38	1.14	3.95
	1–2	−0.91	0.05	0	−16.7	7.61	5.19
	2–3	0.32	0.12	0	−16.6	8.7	4.79
	3–4	0.51	0.26	0	−16.63	7.52	5.01
	4–5	0.41	0.2		−16.65	9.65	5.03
	5–6	0.28	0.06	0	−16.55	10.34	5.15
	6–7	0.17	0.13	0	−16.58	11.4	5.49
	7–8	−0.27	0.03	0	−16.53	6.38	4.86
	8–9	−0.56	0	0	−16.78	4.41	4.59
	9–10	−0.85	0.09	0	−16.4	3.56	4.84
	10–11	−0.85	0.07	0	−16.48	3.19	4.5
	11–12	−0.97	0.03	−0.13	−16.55	3.25	4.42
	12–13	−1.33	0.04	0	−16.5	3.56	5.3
	13–14	−0.95	0.08	0	−16.6	3.69	4.56
	14–15	−1.1	0.08		−16.48	3.44	4.74
	15–16	0.31	0.03	0	−16.68	28.63	8.43
	16–17	2.9	0.01	0	−16.7	79.44	19.66
	17–18	15.49	0	0	−16.6	306.75	72.84
	18–19	4.57	0.03	0	−16.6	94.38	23.31
	19–20	8.08	0	0	−16.7	107.03	29.78
	20–21	10.05	0.03	0.1	−16.7	150.2	37.83
	21–22	7.83	0.09	−0.08	−16.75	122.11	30.19
	22–23	4.42	0.04	0	−16.6	86.11	21.34
	23–24	4.05	0.08	0	−16.45	78.86	19.72

Table 9.10 Characteristics of response in average turbidity for each scenario

Scenarios		Time to response[1] (Hours after blasting)	Maximum response (NTU)	Time to maximum response (Hours after blasting)	Duration of response (Hours)
No precipitation within 24 h after blasting	No precipitation 1 day prior to blasting	0–1	1.5	5–6	22
	No precipitation 5 days prior to blasting	0–1	1.39	5–6	18
	With precipitation 5 days prior to blasting	–[2]	–	–	–
	No precipitation 30 days prior to blasting	0–1	0.33	5–6	18
	With precipitation 30 days prior to blasting	2–3	0.88	3–4	6
With precipitation within 24 h after blasting	No precipitation 1 day prior to blasting	2–3[3]	28.83	17–18	22
	With precipitation 1 day prior to blasting	2–3	0.90	6–7	6
	No precipitation 5 days prior to blasting	0–1	6.08	5–6	17
	With precipitation 5 days prior to blasting	2–3[4]	10.05	20–21	22
	With precipitation 30 days prior to blasting	2–3[5]	14.67	17–18	22

Notes
(1) The response is considered to be positive when two consecutive average turbidity changes are greater than 0.
(2) The average turbidity change is greater than 0 at the first hour. Because the turbidity changes in the remaining 23 h are negative, the positive point was considered to be anomalous.
(3) The average turbidity change is greater than 0 in two separate time periods that is divided by negative changes. The duration is the response time to the end of the 24 h after the blasting.
(4) The average turbidity change is greater than 0 in two separate time periods that is divided by negative changes. The duration is the response time to the end of the 24 h after the blasting.
(5) The average turbidity change is greater than 0 in two separate time periods that is divided by negative changes. The duration is the response time to the end of the 24 h after the blasting.

Because only 4 events are available for this scenario, the statistical results may not represent a full range of conditions, such as the quantity of dynamite in the blasts, the bench level of the blasting, and the number of blast holes. The scenario, in which there were no precipitation activities 5 days prior to blasting and no precipitation within 24 h after blasting, was also used for the blasting impact analysis. The precipitation impact that occurred 6 days prior to blasting could be reasonably considered to be minimal. In this scenario 34 blasting events are available. The average hourly turbidity prior to blasting is 1.58 NTU, which is slightly higher than the previous value of 1.44 NTU. The turbidity change has a positive response in the first hour after blasting and the response lasts approximately 18 h. The magnitude of the response is less than 2 NTU, with a range from 0.03 to 1.39 NTU. The maximum response occurs 5–6 h after blasting. For any particular blasting event out of the 34 events, the turbidity change could be up to 35.04 NTU, which also occurred 5–6 h after blasting.

The scenario, in which there was no precipitation 1 day prior to blasting and no precipitation within 24 h after blasting, may provide the upper limits of the blasting impact on turbidity at SP-1 Spring, because the turbidity values may be impacted by both precipitation 2 days prior to blasting and the blasting itself. In this scenario 57 blasting events are available. The average hourly turbidity prior to blasting is 1.68 NTU. The turbidity change has a positive response in the first hour after blasting and the response lasts approximately 22 h. The magnitude of the average response is also less than 2 NTU, with a range from 0.06 to 1.50 NTU. The maximum response occurs 5–6 h after blasting. For any particular blasting event out of the 57 events, the turbidity change could be up to 36.62 NTU, which occurred 2–3 h after blasting.

The quantitative analysis indicates that the impact of blasting in the quarry on the turbidity at SP-1 Spring is likely no more than 2 NTU. The impact can occur in the first hour after blasting and reach a maximum 5–6 h later. The duration of the impact is approximately 22 h. These statistical conclusions are based on the data available in each scenario and they may not be applicable to any one particular blasting event because other factors may also impact the turbidity values at SP-1 Spring.

9.8.4 Impact of Precipitation on Turbidity at SP-1 Spring

The impact of precipitation on turbidity at SP-1 Spring is obvious when the precipitation occurred either prior to blasting or after blasting. In the scenario in which precipitation occurred within 24 h after blasting and no precipitation occurred 1 day prior to blasting, the turbidity change is 28.83 NTU based on 10 blasting events. Of the 10 blasting events, the turbidity change could reach up to 306.75 NTU in one particular event.

When precipitation occurred within 24 h after and 1 day prior to blasting, the turbidity change is relatively small, up to 0.9 NTU based on 9 blasting events. This is because the rainfall prior to blasting had already elevated the turbidity at SP-1 Spring.

When there was no precipitation within 24 h after blasting but rainfall occurred 1 day prior to blasting, 23 of the 24 turbidity changes are less than 0 based on 18 blasting events. The elevated turbidity caused by the rainfall 1 day prior to blasting clearly masked any impact caused by blasting. The average hourly turbidity prior to blasting is 4.18 NTU. The range of the turbidity change is from −4.98 to −2.49 NTU.

The masking effect is also present in the scenario, in which there was no precipitation within 24 h after blasting but rainfall occurred 5 days prior to blasting, albeit the effect is subdued. There are 51 blasting events that fall into this scenario. All the turbidity changes calculated for this scenario are less than 0, with the minimum being −2.00 NTU.

The masking effect of rainfall on turbidity at SP-1 Spring is further reduced when there was no precipitation within 24 h after blasting but rainfall occurred 30 days prior to blasting. There are 98 blasting events available for this scenario. The turbidity changes include values less than 0 and greater than 0. The positive values occurred 2–8 h after blasting. It seems that both precipitation 30 days prior to blasting and the blasting itself have some impacts on the turbidity at SP-1 Spring. When the precipitation 30 days prior to blasting has more significant impact than blasting, the turbidity changes are less than 0. Otherwise, the blasting impact would overcome the masking effect of precipitation on the turbidity and the turbidity changes would be positive. Overall, the impact of precipitation 30 days prior to the blasting is minimal but seems to be comparable in magnitude to the effect of blasting on the turbidity at SP-1 Spring. Obviously if these data were broken down into finer time increments, one could determine at what point the effects of blasting exceed the residual masking effect of the precipitation.

In order to further study the impact of rainfall on the turbidity at SP-1 Spring without the interference from blasting, the rainfall events that occurred 48 h prior to and after the blasting events were selected. Forty-six rainfall events are available from November 1997 to June 2004. Table 9.11 shows the selected events and their turbidity information. The average turbidity values range from 0.5 to 129.32 NTU, with an average of 14.12 NTU.

The quantitative analysis indicates that precipitation is a major factor that affects the turbidity at SP-1 Spring. Precipitation, either prior to or after blasting, impacts the turbidity changes. It should be pointed out that the turbidity at SP-1 Spring can be affected by many other factors such as logging, construction, and clearing in the spring catchment basin, and the transport characteristics of the sediments in the marble aquifer, above and beyond the two factors analyzed in this study. In addition, the turbidity values used in this study are hourly averages. More frequent measurements in turbidity values may show higher change in magnitude, and less frequent measurement may show lower change in magnitude. For example, if the analysis were performed using the turbidity values every 15 min, the turbidity change might be higher than the results obtained from the hourly averages; however turbidity spikes that only lasted minutes would have only minor impact. On the other hand, the turbidity change would be smaller if daily averages were used.

Based on the statistical analysis from the data available, the preliminary conclusions can be obtained as follows:

- Precipitation is the most important factor that impacts turbidity at SP-1 Spring. Unconsolidated particles are transported mainly during flood flow episodes in response to rainfall events. When water velocities decrease following a storm event, the sediments in suspension may settle out and temporarily be stored in the aquifer. Very small particles, mainly clay or silt, are transported in suspension in the water in between precipitation events. Some small particles may be rolled

Table 9.11 Rainfall events and their impacts on turbidity at SP-1 spring

Rainfall information				Turbidity data at SP-1 spring			
Beginning time (m/d/y hh:mm)	Ending time (m/d/y hh:mm)	Total rainfall (inch)	Average intensity (inch/h)	Background (NTU)	Minimum (NTU)	Maximum (NTU)	Average (NTU)
1/6/1998 20:00	1/20/1998 1:00	9.72	0.0307	2	0.5	204	81.24
1/26/1998 14:00	2/10/1998 20:00	12.74	0.0348	204	9.25	204	129.32
2/13/1998 4:00	3/3/1998 3:00	5.46	0.0134	9.42	8.58	204	50.76
3/11/1998 15:00	3/13/1998 15:00	0.49	0.0204	15.33	15.33	29.33	19.94
11/23/1998 13:00	11/30/1998 19:00	4.27	0.0245	0.5	0.2	3.28	0.5
1/15/1999 2:00	1/26/1999 14:00	15.36	0.0557	0.73	0.45	162.15	18.63
1/30/1999 23:00	2/1/1999 9:00	1.19	0.035	1.6	1.5	1.9	1.69
2/6/1999 10:00	2/10/1999 11:00	9.6	0.099	1.77	1.57	176.37	15
2/13/1999 17:00	2/13/1999 23:00	0.35	0.0583	3.25	1.65	3.28	2.45
2/16/1999 5:00	2/22/1999 6:00	4.4	0.0303	1.9	1.6	63.53	9.62
2/24/1999 23:00	2/26/1999 14:00	0.79	0.0203	1.75	1.58	1.85	1.74
3/1/1999 1:00	3/3/1999 6:00	0.7	0.0132	1.8	1.75	2.1	1.98
3/8/1999 13:00	3/11/1999 8:00	1.52	0.0227	1.68	1.73	16.88	4.1
3/14/1999 5:00	3/25/1999 6:00	4.87	0.0184	1.85	1.5	4.28	1.88
3/30/1999 20:00	3/31/1999 9:00	0.52	0.04	2.1	1.98	2.05	2.03
4/5/1999 8:00	4/12/1999 8:00	4.04	0.024	2	1.8	52.2	4.59
5/2/1999 19:00	5/3/1999 15:00	0.28	0.014	0.95	0.85	1.45	0.92
5/30/1999 8:00	6/3/1999 10:00	0.53	0.0054	0.78	0.73	1.18	0.84
9/8/1999 17:00	9/9/1999 4:00	0.18	0.0164	0.95	0.93	1.3	1.01

(continued)

Table 9.11 (continued)

Rainfall information				Turbidity data at SP-1 spring			
Beginning time (m/d/y hh:mm)	Ending time (m/d/y hh:mm)	Total rainfall (inch)	Average intensity (inch/h)	Background (NTU)	Minimum (NTU)	Maximum (NTU)	Average (NTU)
1/1/2000 14:00	1/1/2000 22:00	0.06	0.0075	0.68	0.63	0.7	0.68
1/11/2000 4:00	1/26/2000 3:00	5.15	0.0143	0.6	0.6	978.4	84.06
1/30/2000 0:00	2/1/2000 0:00	1.55	0.0323	4.78	3.35	4.85	3.89
12/13/2001 20:00	12/14/2001 14:00	0.89	0.0494	5.25	5.13	9.81	6.04
12/16/2001 23:00	12/17/2001 10:00	1.15	0.1045	2.94	0.94	35.5	5.56
12/21/2001 16:00	12/23/2001 5:00	0.89	0.0241	21.88	9.63	46.63	17.45
12/27/2001 16:00	1/3/2002 3:00	7.51	0.0485	1.94	0.13	1000.56	118.46
1/21/2002 14:00	1/22/2002 0:00	0.15	0.015	0.94	0.94	3.25	2.03
1/26/2002 4:00	1/29/2002 12:00	1.1	0.0138	4.75	0.94	5.5	2.62
2/16/2002 16:00	2/20/2002 2:00	2.04	0.0249	5.56	1.75	114.38	9.41
3/6/2002 0:00	3/7/2002 15:00	1.06	0.0272	2.5	2.06	13.38	3.49
3/10/2002 0:00	3/10/2002 8:00	0.52	0.065	2.56	1.94	6	2.87
3/15/2002 16:00	3/17/2002 16:00	0.61	0.0127	2.56	2.06	8.69	2.83
4/4/2002 8:00	4/5/2002 15:00	0.07	0.0023	2.38	2.13	3	2.55
4/22/2002 17:00	4/26/2002 10:00	0.23	0.0026	2.56	2.5	2.69	2.6
5/15/2002 1:00	5/16/2002 22:00	0.83	0.0184	2.75	2.25	2.75	2.52
11/14/2003 14:00	11/18/2003 1:00	0.81	0.0098	1.6	1.6	1.6	1.6
11/30/2003 3:00	12/7/2003 8:00	4.29	0.0248	1.6	0.23	4.33	1.39
12/19/2003 15:00	1/2/2004 20:00	12.42	0.0365	0.31	0.08	190.11	5.01

(continued)

Table 9.11 (continued)

Rainfall information				Turbidity data at SP-1 spring			
Beginning time (m/d/y hh:mm)	Ending time (m/d/y hh:mm)	Total rainfall (inch)	Average intensity (inch/h)	Background (NTU)	Minimum (NTU)	Maximum (NTU)	Average (NTU)
1/6/2004 21:00	1/10/2004 4:00	0.7	0.0089	2.81	1.6	11.94	4.98
1/13/2004 3:00	1/15/2004 4:00	0.06	0.0012	1.6	1.52	1.6	1.58
1/19/2004 2:00	1/21/2004 2:00	0.03	0.0006	1.6	1.6	1.6	1.6
1/24/2004 0:00	1/24/2004 10:00	0.68	0.068	1.6	1.45	3.58	1.75
1/26/2004 18:00	2/4/2004 5:00	3.46	0.0171	1.6	1.29	96.08	8.57
2/6/2004 20:00	2/6/2004 23:00	0.05	0.0167	1.6	1.52	1.6	1.57
2/16/2004 0:00	2/27/2004 14:00	4.99	0.0179	1.68	1.45	81.41	4.44
4/19/2004 2:00	4/21/2004 11:00	0.75	0.0132	1.6	1.6	1.75	1.66

along the bottom of the conduits by the water flowing over the particles. Precipitation can cause an elevation in turbidity of 14.12 NTU on average, with a range from 0.5 to 129.32 NTU.

- The blasting activities in the quarry have some impacts to SP-1 Spring. Blasting has the potential to elevate the turbidity at SP-1 Spring by less than 2 NTU on an average basis. Its maximum response tends to occur 5–6 h after blasting, and the impact can last up to 22 h.

9.9 Conclusions

The study area has very complex geology and hydrogeology and has a well-developed karst terrane characterized by sinkholes, sinking streams, caves and large springs in marble. The subsurface in the karst land consists of two distinctive zones—the deeper saturated zone (karst aquifer) and the overlying unsaturated zone (perched aquifer). The unsaturated zone has a high capacity for storing water temporarily, and it has a poor hydraulic connection with the saturated zone. The saturated water level in the saturated zone at the projected bottom of the quarry in the amendment area is below 741 feet amsl, according to the water levels measured in M1B in 2003 and 2004. The unsaturated zone can be over 300 feet thick.

The karst aquifer that feeds SP-1 Spring is well developed. Water flows through discrete solution-widened fractures/conduits in the saturated zone at estimated flow rates from 20 feet/day to 2560 feet/day. More than one conduit system may exist, and the conduits tend to be larger as they are closer to SP-1 Spring. Monitoring wells M1B and NZA likely intercepted, or are very close to, the conduits in the aquifer.

The karst aquifer receives recharge from allogenic as well as autogenic sources. Allogenic recharge is from the borderlands, including sinking streams SS-8, SS-1, SS-2, and SS-4, sinkhole plain, and the landslide deposits. The autogenic recharge is from the karst land including the existing quarry and the amendment area. The total delineated catchment area for SP-1 Spring is approximately 2000 acres. Allogenic recharge accounts for approximately 90% of the total catchment area; whereas autogenic recharge accounts for approximately 10% of the total catchment area. The recharge sources for SP-1 Spring are predominantly allogenic.

Turbidity increase in response to rainfall events is typical of well-developed karst springs and SP-1 Spring is no exception. The turbidity response of SP-1 Spring to rainfall is predominantly caused by the multiple allogeneic recharge sources, especially recharge from sinking streams SS-1 and SS-2, the sinkhole plain, and the landslide deposits. Transport of sediment particles through conduit systems and discharge of the sediments at springs are essential functions of a karst aquifer. In well-developed aquifers like the one under study, where surface streams sink underground, the insoluble materials carried by the sinking surface streams are carried through the conduit system and washed out through the springs. If the flow is not sufficient to remove sediments from conduits or fractures, the karst aquifer will eventually become plugged.

The discharge of SP-1 Spring in response to rainfall is predominantly caused by allogenic recharge. The characteristics of the response may depend on the sources that dominate a particular recharge event. It takes approximately one to two weeks for the majority of water recharged at sinkhole SH-11, sinking streams SS-1 and SS-2 to arrive at SP-1 Spring, whereas it takes approximately 3 months for the majority of water recharged at sinking streams SS-8 and SS-4 to reach SP-1 Spring.

Multivariate statistical analysis further substantiates the fact that precipitation is the most important factor impacting the turbidity at SP-1 Spring. Rainfall events can raise the turbidity level of 14.12 NTU on average, with a range from 0.5 to 129.32 NTU, whereas the "background" turbidity, in the absence of rainfall, is approximately 1.44 NTU. Unconsolidated particles are transported mainly during flood flow episodes in response to rainfall events. The blasting activities in the quarry may elevate the turbidity at SP-1 Spring by less than 2 NTU on an average basis. Its maximum response tends to occur 5–6 h after blasting and the impact lasts 22 h.

References

Abkemeier TJ, Stephenson RW (2003) Remediation of a Sinkhole Induced by Quarrying, in Sinkholes and the Engineering and Environmental Impacts of Karst, Proceedings of the Ninth Multidisciplinary Conference, Sept. 6–10, 2003, Huntsville, Alabama, Beck, BF (ed.) Geotechnical Special Publication No. 122, ASCE, pp 605–614

Akers JP, Jackson LE Jr (1977) Geology and ground water in western Santa cruz county, California, with particular emphasis on the Santa margarita sandstone: U.S. geological survey water resources investigation, 77–15 open file report

Alexander EC Jr, Quinlan JF (1992) Practical tracing of groundwater with emphasis on karst terranes, 2nd edn. Geological Society of America, Boulder CO, Short Course Manual

Aley T (1999) Groundwater tracing book. The Ozark Underground Laboratory, MO, p 33p

ASTM (American Society for Testing and Materials) (1998) ASTM D 6312-98, Standard guide for developing appropriate statistical approaches for ground-water detection monitoring programs. annual book of standards, West Conshohocken, PA. pp 1–14

Atteia O, Kozel R (1997) Particle size distributions in waters from a karstic aquifer: from particles to colloids. J Hydrol 201:102–119

Brabb EE (1989) Geologic map of santa cruz county, California: U.S. Geological survey miscellaneous investigation series maps I-1905

Bretz JH (1964) Vadose and phreatic features of limestone caves. J Geol 675–811

Clark JC (1981) Stratigraphy, paleontology, and geology of the central Santa cruz mountains. U.S. Geological Survey Professional Paper, California Coast Ranges

Crawford Hydrology Lab (2003) Laboratory procedure and quality assurance/quality control plan. Western Kentucky University, Bowling Green, KY

Drever JI (1997) The geochemistry of natural waters, 3rd edn. Prentice Hall, NJ, p 436

EPA (1989) Statistical analysis of ground-water monitoring data at RCRA facilities. interim final guidance, EPA/530-SW-89-026, Washington DC: office of solid waste, U.S. Environmental Protection Agency

EPA (1992) Statistical analysis of ground-water monitoring data at RCRA facilities: addendum to interim final guidance, in statistical training course for ground-water monitoring data analysis. EPA530-R-93-003

EPA (1996) Guidelines for wellhead and springhead protection area delineation in carbonate rocks: environmental protection agency, region 4, U. S. EPA 904-B-97–003. Prepared by Eckenfelder, Inc., Nashville, TN

EPA (Environmental Protection Agency) (2002) The QTRACER2 program for tracer-breakthrough curve analysis for tracer tests in karstic aquifers and other hydrologic systems: national center for environmental assessment—Washington Office, EPA/600/R-02/001

Even H, Carmi I, Magaritz M, Gerson R (1986) Timing the transport of water through the upper vadose zone in a karstic system above a cave in Israel. Earth Surf Proc Land 11:181–188

Field MS (2002) A review of some tracer-test design equations for tracer-mass estimation and sample-collection frequency. Environ Geol 43:867–881

Field MS, Wilhelm RG, Quinlan JF, Aley TJ (1995) An assessment of the potential adverse properties of fluorescent tracers dyes used for groundwater tracing: environmental monitoring and assessment. 38:75–96

Foose RM (1953) Ground-water behavior in the Hershey Valley, Pennsylvania. Geol Soc Am Bull 64:623–645

Fournie M, Massei N, Bakalowicz M, Dussart-Baptista L, Rodet J, Dupont JP (2007) Using turbidity dynamics and geochemical variability as a tool for under-standing the behavior and vulnerability of a karst aquifer. Hydrogeol J 15:689–704

Green JA, Pavlish JA, Leete JH, Alexander EC, Jr (2003) Quarrying impacts on groundwater flow paths. In: Beck BF (ed) Ninth Multidisciplinary Conference on Sinkholes and the Engineering and Environmental Impacts of Karst. Geotechnical Special Publication No. 122, pp 216–222

Gunn J (1986) A conceptual model for conduit flow dominated karst aquifer. In: Gunay G, Johnson AI (eds) Proceedings of karst water resources conference in Ankara, Turkey. International association of hydrological sciences. pp 587–596

Hubbard EF, Kilpatrick FA, Martens LA, Wilson JF Jr (1982) Measurement of the time of travel and dispersion in streams by dye tracing: U.S. Geological survey techniques of water-resources investigations, Book 3, Chapter A9, p 44

Käss W (1998) Preparation and realization of tracing tests. In: Käss W (ed) Tracing technique in geohydrology, A.A. Balkema, Rotterdam, Netherlands. p 315–39

Lolcama JL, Cohen HA, Tonkin MJ (1999) Deep karst conduits, flooding, and sinkholes: Lessons for the aggregates industry. Eng Geol 65(2–3):151–157

Mahler BJ, Lynch FL (1999) Muddy waters: temporal variation in sediment discharging from a karst spring. J Hydrol 214:165–178

McCarthy JF, Schevenell LS (1998) Processes controlling colloid composition in a fractured and karstic aquifer in eastern tennessee USA. J Hydrology 206:191–214

Mull, DS, Liebermann, TD, Smoot, JL, and Woosley, LH (1988) Application of dye-tracing techniques for determining solute-transport characteristics of ground water in karst terranes: U.S. Environmental protection agency, EPA 904/6-88-001. p 103

Ongley E (1996) Sediment measurements, Chapter 13. In: Bartran J, Balance R (eds) Water quality monitoring—A practical guide to design and implementation of freshwater quality studies and monitoring programs, UNEP/WHO

Phillips LR (1990) Depositional and structural controls on the distribution of tar sands in the Santa cruz mountains, California. In: Greene HG (eds) Geology and tectonics of central California coast region, San Francisco to monterey. Pacific Section AAPG Book GB67

Quinlan JF (1986) Water-tracing techniques in karst terranes: practical karst hydrogeology with emphasis on groundwater monitoring, a short course. National Water Well Association, Dublin, Ohio, p 25

Shevenell LS, McCarthy JF (2002) Effects of precipitation events on colloids in a karst aquifer. J Hydrology 255:50–68

Smart PL (1984) A review of the toxicity of twelve fluorescent dyes used for water tracing: national speleological society. Bulletin 46:21–33

Smart PL, Laidlaw IMS (1977) An evaluation in some fluorescent dyes used for water tracing. Water Resour Res 13:15–33

Sutter RD, Verhoeven R (2001) Simulation of sediment transport during flood events: laboratory work and field experiments. Hydrol Sci 46(4):559–610

Todd D (1963) Ground water hydrology of the bonnie doon quarry site, Santa cruz county. California. Prepared for Wisser and Cox, Berkeley, CA

Townsend MA, Macfarlane PA (2003) Seasonality effects on karst aquifers, flint hills region, central Kansas, Kansas geological survey. In: Beck BF (ed) Sinkholes and the engineering and environmental impacts of Karst, geotechnical special publication #122, ASCE. pp 277–286

Valdes D, Dupont J-P, Massei N, Laignei B, Rodet J (2005) Investigation of karst hydrodynamics and organization using autocorrelations and T-C curves. J Hydrol 329:432–443

White WB (1988) Geomorphology and hydrology of karst terrains. Oxford, New York, p 464p

White WB (1993) Analysis of karst aquifers. In: Alley WM (ed) Regional ground-water quality. Van Nostrand Reinhold, New York

Williams PW (1985) Subcutaneous hydrology and the development of dolin and cockpit karst. J Geomorphol 29:463–482

Wisser and Cox (1960) Groundwater conditions of quarry site, Santa cruz county. California, San Francisco, CA

Worthington SRH, Smart CC (2003) Empirical determination of tracer mass for sink to spring tests in karst. In: Beck BF (ed) Sinkholes and the engineering and environmental impacts of karst. ASCE geotechnical special publication No. 122